Cell Calcium 133 (2026) 103091

Contents lists available at ScienceDirect

Cell Calcium

journal homepage: www.elsevier.com/locate/ceca

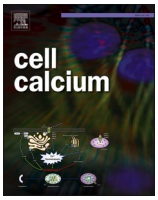

Fura-10, unlike fura-2, is suitable for long-term calcium imaging in natural killer (NK) cells without compromising cytotoxicity and can be combined with target cell death analysis

Lea Kaschek [a,1,*], Joanne Vialle [a,1], Gebhard Stopper [a,1], Markus D.A. Hoffmann [b], Sylvia Zöphel [a], Johanna Jansky [a], Nadja Küchler [a], Gertrud Schäfer [a], Alina Moter [c,d], Philipp Wendel [c,d,e,f], Frank Neumann [g], Claudia Schormann [g], Evelyn Ullrich [c,d,e], Leticia Prates Roma [b], Carsten Kummerow [a], Lorenz Thurner [g], Eva C. Schwarz [a], Markus Hoth [a,*]

[a] Biophysics, Center for Integrative Physiology and Molecular Medicine (CIPMM), School of Medicine, Saarland University, 66421 Homburg, Germany
[b] Biophysics, Center for Integrative Physiology and Molecular Medicine (CIPMM) and Center of Human and Molecular Biology (ZHMB), School of Medicine, Saarland University, 66421 Homburg, Germany
[c] Goethe University Frankfurt, Department of Pediatrics, Experimental Immunology and Cell Therapy, Frankfurt (Main), Germany
[d] Goethe University Frankfurt, Frankfurt Cancer Institute (FCI), Frankfurt (Main), Germany
[e] German Cancer Consortium (DKTK), Partner Site Frankfurt/Mainz and German Cancer Research Center (DKFZ), Heidelberg, Germany
[f] Institute for Organic Chemistry and Biochemistry, Technical University of Darmstadt, Darmstadt, Germany
[g] Internal Medicine I, School of Medicine, Saarland University, 66421, Homburg, Germany

ARTICLE INFO

Key words:
Natural killer (NK) cell
Fura-10
Fura-2
Calcium
Cytotoxicity
cancer
Pancreatic islets

ABSTRACT

There are compelling reasons to opt for primary human natural killer (NK) cells when validating Ca^{2+} indicators. 1.) NK cells exhibit a high degree of vulnerability to stressors such as indicator loading or light exposure. 2.) The lack of research on NK Ca^{2+} signaling underscores the necessity for developing reliable assays. 3.) The increased utilization of NK cell therapies necessitates a more profound comprehension of Ca^{2+} dependent signal transduction. Consequently, an assay was developed to monitor cytosolic Ca^{2+} signals in individual NK cells simultaneously with their cytotoxic function against cancer cells. We used this assay to assess the suitability of fura-2, fura-PE3, fura-8, fura-10 or fura-red for quantifying Ca^{2+} signals in NK cells without compromising their cytotoxic function. In contrast to the widely used fura-2, its red-shifted derivative fura-10 did not interfere with NK cytotoxicity over several hours. It exhibited a superior signal-to-noise ratio and good dynamic range, accompanied by minimal bleaching or leakage. Fura-8 and fura-red also preserved NK cell cytotoxicity, but had other disadvantages compared to fura-10. We successfully used fura-10 to report Ca^{2+} signals in NK cells from blood donors and patients diagnosed with lymphoma and leukemia over several hours at 37 °C during apoptotic or necrotic killing of different cancer cells (K562, THP1, OCI-AML2, and TMD8). Additionally, we show that fura-10 is well suited to report Ca^{2+} signals in intact murine pancreatic islets, another stress-sensitive cell preparation. Consequently, fura-10 is an optimal choice for measuring Ca^{2+} in primary human NK cells and other primary cell preparations.

1. Introduction

Many cellular functions are tightly linked to Ca^{2+} signaling. To better understand these processes, it is important to investigate Ca^{2+} signals in single cells over extended periods of time. Determining whether any given process in cells is Ca^{2+} dependent or not is relatively straightforward. This is usually achieved by altering intracellular Ca^{2+} concentrations in vitro and monitoring the resulting changes by synthetic [1] or genetically encoded Ca^{2+} indicators (GECI) [2], which both can be intensity-based or ratiometric. Ratiometric indicators are usually

* Corresponding authors at: Biophysics, Center for Integrative Physiology and Molecular Medicine (CIPMM), Building 48, School of Medicine, Saarland University, 66421 Homburg, Germany.
E-mail addresses: lea.kaschek@uni-saarland.de (L. Kaschek), markus.hoth@uks.eu (M. Hoth).
[1] Contributed equally

https://doi.org/10.1016/j.ceca.2025.103091
Received 2 October 2025; Received in revised form 19 November 2025; Accepted 20 November 2025
Available online 21 November 2025

preferred because they can report quantitative Ca^{2+} signals with higher fidelity.

In murine cells and in cell lines, the choice of indicators is often not restricted. Arguments for GECIs in transgenic models or cell lines are plentiful: stable expression can be easily achieved, and they are often believed to be less toxic than synthetic indicators [3,4]. Nevertheless, synthetic indicators are still commonly used due to their uncomplicated application, superior signal-to-noise (or signal-to-background) ratio and the higher dynamic range when compared to genetically encoded indicators.

Measuring Ca^{2+} in primary human cells is more challenging. Inefficient transfection and cell stress after harsh transfection routines make the use of GECIs more difficult, whereas synthetic Ca^{2+} indicators bear higher risks of toxicity.

The majority of Ca^{2+} measurements by microscopy including the ones in primary human immune cells are carried out with fura-2, which is by far the most widely used ratiometric Ca^{2+} indicator since its groundbreaking introduction by the Tsien lab [1]. Most flow cytometric measurements are performed using fluo derivatives (intensity-based) or indo-1 (ratiometric).

In particular, the far UV wavelength of 340 nm used for fura-2 excitation has been discussed to be harmful to cells considering that UV radiation induces cell damage followed by damage-induced signaling events [5]. Recently, Robinson et al. have presented clear evidence that Ca^{2+} measurements with fura-2 and fluo-4 impair contractility of primary murine and human induced pluripotent stem cells [3]. In addition, Zhou et al. have pointed out difficulties in using fura-2 with light-emitting diodes in commercial microscopes and presented a new red shifted ratiometric Ca^{2+} indicator called isoCaRed-1Me [6]. Furthermore, BAPTA-derived Ca^{2+} indicators like fura-2, fluo-4 or rhod-2 are known to have side effects like inhibiting the Na^+/K^+ ATPase [7,8]. Therefore, it appears important to control cell functionality when using Ca^{2+} indicators, in particular if Ca^{2+} needs to be measured over extended times.

Natural killer (NK) cells are one of the major classes of cytotoxic immune cells. They are important to eliminate cancer and virus-infected cells. NK cells kill cancer cells which have lost MHC (major histocompatibility complex) class I molecules but also recognize stressed cells including MHC class I-positive cancer cells through interactions with their activating and inhibitory surface receptors [9]. NK cytotoxicity is modulated by activating (e.g., IL-2, IL-12, IL-15) and inhibitory (e.g., TGF-β, IL-10) cytokines, released by immune cells present in the tumor-immune environment including NK cells themselves. Cytotoxicity is mediated by various mechanisms including release of perforin and granzymes from lytic granules and activation of death receptors (Fas and TRAIL-R) on cancer cells [9]. Knocking out different surface receptors revealed NK cells' crucial role for tumor surveillance [10]. Among different signaling cascades, Ca^{2+} signaling is important for cytotoxic functions of NK cells [11–13].

When compared to other immune cells, however, reports about Ca^{2+} measurements in primary human or murine NK cells are extremely sparse. The reason for the lack of Ca^{2+} data is unclear. Our PubMed search revealed only 14 publications reporting Ca^{2+} measurements via flow cytometry and just nine using microscopy. It is, of course, possible that we have inadvertently overlooked publications. Nevertheless, numbers are very low. Flow cytometry measurements were carried out using fura-red, indo-1, or various fluo indicators [13–26]. For microcopy, fura-2 was the dominant indicator [27–30], followed by fluo derivatives [31–33], a combination of fura-red and fluo4 [26], or indo-1 [34]. Some Ca^{2+} measurements with photomultipliers, the FLIPR 6-QF Ca^{2+} kit, spectrometers or the isotope Ca-45 are also reported [35–40]. Among these studies, only few were performed at physiological temperature of 37 °C: one using both microscopy and flow cytometry by Bryceson et al. [26], two flow cytometry studies by Ganesan and Hoglund [14,15] and one study using a spectrometer [39]. Additionally, a fourth study reported measurements at 35 °C [35]. All remaining studies were performed at room temperature (usually around 22 °C) which is problematic considering the strong dependence of Ca^{2+} signals on temperature [41].

NK cell function is highly sensitive to experimental conditions, making them an optimal system for assessing the potential toxicity of Ca^{2+} indicators, similar to primary cardiomyocytes [3]. Currently, different NK cell types, such as chimeric antigen receptor NK (CAR-NK) cells, allogeneic induced pluripotent stem cell (iPSC)-derived NK cells, autologous NK cells or NK-92 cells, are being tested for cancer treatment [42]. A detailed characterization of NK signalling and cytotoxicity would help to optimize personalized treatment of patients. As Ca^{2+} signaling is crucial for NK cytotoxicity [13,30], further investigation into NK cell Ca^{2+} signaling is warranted. For these reasons, the objective of this study was to test ratiometric Ca^{2+} indicators in natural killer (NK) cells, with the overarching goal of preserving long-term NK cell functionality.

2. Results

2.1. Characterization of ratiometric Ca^{2+} indicators in primary human NK cells

Our aim is to identify Ca^{2+} indicators to measure Ca^{2+} signals in single primary human NK cells over several hours while maintaining their functionality against target cells. For our specific case, we aim to correlate Ca^{2+} levels in NK cells with the death of their cancerous target cells. We use the GFP-FRET based apoptosis-reporter pCasper to classify target cell death [43,44]. For Ca^{2+} measurements, we did not consider non-ratiometric indicators as they are not well-suited for long-term experiments, nor did we consider genetically encoded indicators because primary human NK cells are very difficult to transfect or infect. In addition, if Ca^{2+} signals have to be analyzed immediately after NK cell preparation, which in some cases is required, it is impossible to wait for indicator expression following genetic modification. Ratiometric fura indicators have been used successfully in many cell types, with fura-2 being the one most frequently used. We chose 5 ratiometric synthetic Ca^{2+} indicators: fura-2, fura-PE3, fura-8, fura-10 and fura-red. We did not consider any other ratiometric Ca^{2+} indicators because of certain limitations. Indo-1 is a ratiometric emission indicator often used in flow cytometry experiments but is more difficult to handle with many microscopes, which are not equipped for fast dual emission, and in addition it is known to bleach faster than fura-2 [45]. Rhod-2 is well-known to accumulate in mitochondria in T cells and other cells [46], a clear disadvantage for cytosolic Ca^{2+} measurements. Quin-2 is relatively dim compared to fura-2 [1], while fura-5 N and fura-FF have a very low Ca^{2+} affinity [47,48]. The recently introduced isoCaRed-1Me [6] was also excluded because its excitation at 475 nm completely overlaps with the excitation wavelength of the pCasper construct expressed in our target cells [44], and the interference would disturb NK cell Ca^{2+} measurements too much when using epifluorescence microscopes, especially when NK and target cells are in close contact.

To characterize the five fura indicators, we first measured their excitation and emission spectra in primary human NK cells (Fig. 1A) within the spectral range indicated in Table 1. To measure spectra of indicators in NK cells with as little Ca^{2+} as possible in the cytosol, we depleted Ca^{2+} stores in 0 mM Ca^{2+} (1 mM EGTA) by thapsigargin and ionomycin for at least 10 min. For spectra in high Ca^{2+}, 20 mM Ca^{2+} was added in the presence of thapsigargin and ionomycin. Measuring in cells is important because spectra in the cytosol of living cells may differ from those acquired of the compound in solution. These measurements were used to choose the most suitable excitation and emission wavelengths which could be achieved with our LEDs and customized bandpass filters. The wavelengths chosen are indicated in the figure and are close to optimal wavelengths provided by the suppliers. Table 2 summarizes the respective LEDs and filters used for each indicator for measurements with the CellObserver microscope. By choosing optimal wavelengths for

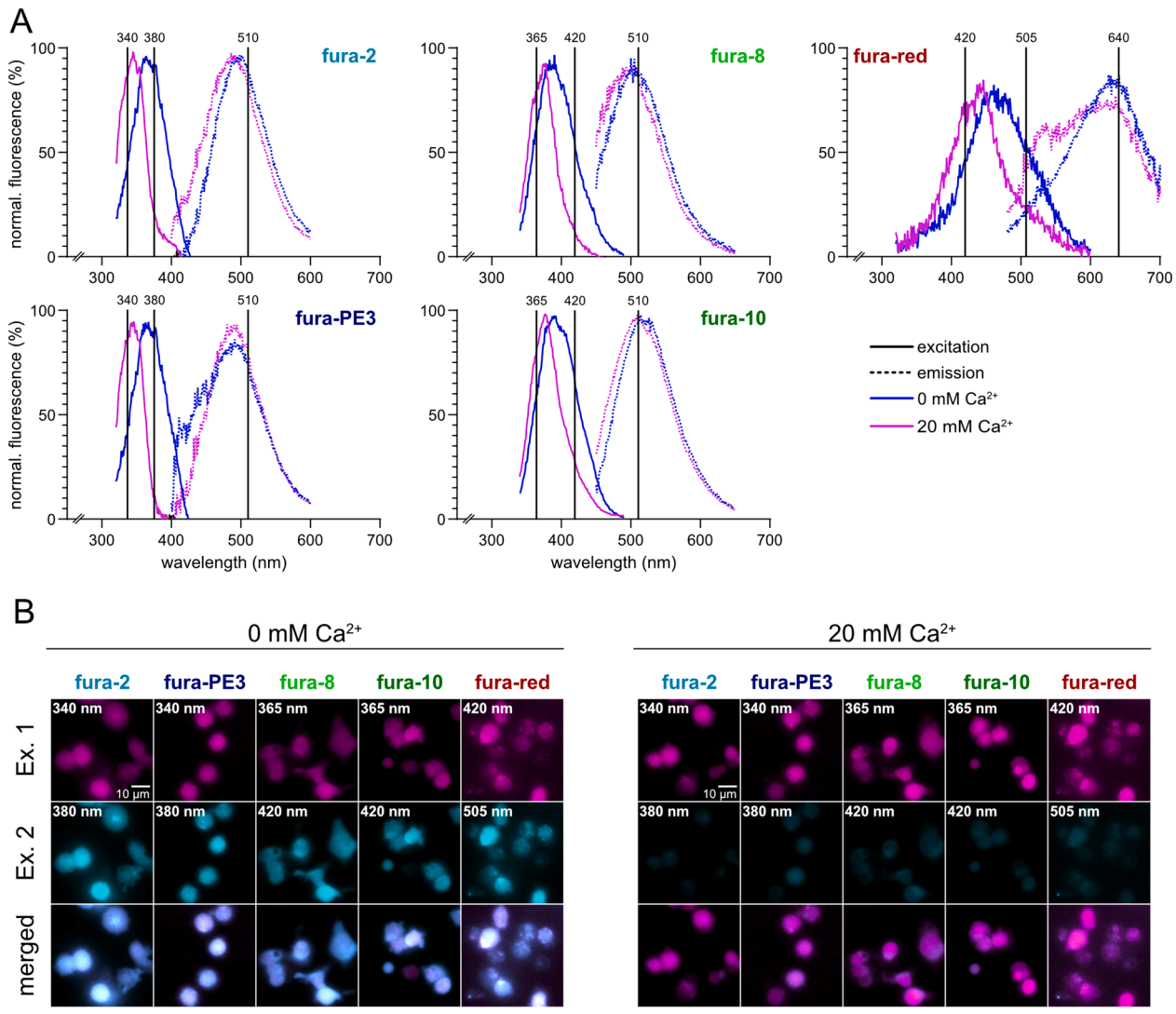

Fig. 1. Spectral properties and indicator loading in primary NK cells. (A) Excitation spectra for Ca^{2+} bound and Ca^{2+} free state (solid lines) and emission (dotted lines) spectra of fura-2-, fura-PE3-, fura-8-, fura-10-, and fura-red-loaded primary NK cells under low-Ca^{2+} (0 mM Ca^{2+}, 1 mM EGTA, blue) or high-Ca^{2+} (20 mM Ca^{2+}, magenta) conditions. Thapsigargin (1 µM) and ionomycin (4 µM) were added to both solutions. Spectra were recorded at 37 °C/5 % CO_2 in the plate reader. Data represent the mean of 5–15 measurements per condition. Vertical bars indicate the excitation and emission wavelengths used in subsequent experiments. (B) Representative images with the Cell Observer (40x) of primary NK cells loaded with each indicator, showing both excitation channels and the corresponding merged images for 0 mM Ca^{2+} and 20 mM Ca^{2+} conditions. Scale bar: 10 µm.

Table 1
Excitation and emission spectra for excitation and emission scans with the CLARIOstar.

Indicator	Excitation (Ex.) scan (nm)	Emission (Em.) scan (nm)
fura-2 and fura-PE3	Ex.: 320/8 to 450/8, Em.: 510/20	Ex.: 360/16, Em.: 400/12 to 600/12
fura-8 and fura-10	Ex.: 340/10 to 490/10, Em.: 522/16	Ex.: 360/16, Em.: 450/10 to 650/10
fura-red	Ex.: 320/10 to 600/10, Em.: 660/16	Ex.: 448/16, Em.: 480/10 to 740/10

Ca^{2+}-bound (referred as excitation wavelength 1) and for the Ca^{2+}-free state (referred as excitation wavelength 2), we could clearly see well-defined cells in the 0 mM Ca^{2+} condition (Fig. 1B). As expected, cells became brighter in the first and dimmer in the second excitation channel by increasing extracellular Ca^{2+} from 0 to 20 mM after activation of store-operated Ca^{2+} entry at 40x magnification (Fig. 1B) and at 63x (Supplementary Figs. 1A, B). In 20 mM Ca^{2+}, cells in excitation channel 2 were generally quite dim, however, they were still well separated from

Table 2
Excitation and emission settings for Ca^{2+} imaging in the Cell Observer.

Indicator	Excitation Ch1 LED (intensity, exposure) + filter	Excitation Ch2 LED (intensity, exposure) + filter	Ch1: Ch2	Beam splitter	Emission filter
fura-2 and fura-PE3	365 nm LED (80 %, 2–300 ms) + 340/30 nm filter	380 nm LED (30 %, 1–150 ms) + 380/10 nm filter	2:1	BS 409 nm	510/90 nm
fura-8 and fura-10	365 nm LED (8 %, 0.15–60 ms) + 370/10 nm filter	420 nm LED (8 %, 0.5–200 ms), no additional filter	1:3,3	BS 458 nm	510/90 nm
fura-red	420 nm LED (30 %, 0.2–60 ms) + 427/15 nm filter	505 nm LED (30 %, 1–300 ms) + 504/17 nm filter	1:5	Triple BS 440, 520, 607 nm	464/18 nm, 542/18 nm, 639/30 nm

the background as shown in Supplementary Fig. 1C for 40x and 63x magnification with brightness of the pictures being increased.

Indicators are often not completely evenly distributed in the cytosol, which is for instance well-known for fura-2 in T cells due to accumulation of indicators in organelles, in case of T cells mainly in mitochondria [49]. This could lead to errors measuring cytosolic Ca^{2+} signals. On average, uneven indicator distribution appeared to be more prominent in fura-2 than in fura-10 (Fig. 1B, Supplementary Fig. 1). For fura-2, we have previously tried to quantify errors of cytosolic $[Ca^{2+}]_{int}$ measurements due to compartmentalization. These errors are not very high but can be completely avoided by using electroporation with fura-salt [49].

An important parameter to consider when choosing indicators is their dynamic range, which is for ratiometric Ca^{2+} indicators defined by dividing the ratio at very high Ca^{2+} by the ratio at very low Ca^{2+}. To determine ratios, IL-2–activated primary NK cells were seeded onto poly-L-lysine–coated coverslips and loaded with the respective Ca^{2+} indicator. Cells were first recorded in 0.5 mM Ca^{2+} buffer to adjust the exposure time ratio of both channels such that the average fura ratio is around 0.5 (Fig. 2A). This ensures that both excitation channels have signals of the same order of magnitude under resting conditions and during stimulation. Measurements of the same cells were then performed in 0.5 mM Ca^{2+} buffer, Ca^{2+}-free buffer (0 mM Ca^{2+}, EGTA) and in high-Ca^{2+} buffer (20 mM Ca^{2+}) (Fig. 2A) to test the respective ratios. Thapsigargin and ionomycin were used to deplete Ca^{2+} stores and were present in 0 mM Ca^{2+} and 20 mM Ca^{2+} buffers. For 0 mM Ca^{2+} ratios were in the range of 0.3 and for 20 mM Ca^{2+} around 2 apart from fura-PE3. The LED intensities used and excitation times of both excitation wavelengths for all five indicators are listed in Table 2.

Ratios of ratiometric indicators and thus also dynamic ranges can be calculated in different ways, focusing on pixel-based (as in Fig. 2A) or average-based methods. Both methods are used in the Ca^{2+} field, and we thus wanted to compare dynamic ranges for both of them. The pixel-based method calculates the ratio of gray values for background-corrected individual pixels and averages all pixels belonging to a single cell using regions of interest (ROIs). The average-based method first averages the fluorescence intensity values of each pixel belonging to a single cell (ROI), then averages both background-corrected channels for all cells and determines average ratios. Both methods should not be mixed because they may lead to different indicator ratios.

The pixel-based method revealed different apparent dynamic ranges for the indicators as calculated from the average ratios of all cells (Fig. 2B). Analyzing the ratios of the individual cells reveals different apparent dynamic ranges for each indicator as shown for the highest exposure time (Fig. 2C) and all exposure times tested (Supplementary Fig. 2). This is not surprising since cells try to avoid very high (toxic) Ca^{2+} signals by extensive pumping, which some cells manage better than others. This means that the actual dynamic ranges of the indicators within cells are probably underestimated because indicator saturation with Ca^{2+} may not be reached in most cells. The dynamic ranges determined by the average-based method (Fig. 2D) revealed similar values for the indicators as the "pixel-based one" ranging from 5 for fura-PE3 to about 8.5 for fura-2.

We noticed that dynamic ranges appeared to be smaller for all indicators at low exposure. This effect was more pronounced in the pixel-based versus the average-based method and may be explained by the nature of ratiometric imaging: When exposures are too short, the measured signals are dominated more by noise rather than true fluorescence. In this case, the fura ratios effectively represent a ratio of noise divided by noise, which approximates 1 when the noise levels are similar in both channels. As noise is a bigger problem for the pixel-based method, it is not surprising that the low exposure effect is more severe in this case.

Another important quality parameter of indicators is the signal-to-background ratio. Our aim was to obtain a signal at least twofold above background, enabling reliable analysis of migrating NK and target cells, when analyzed automatically. Figs. 2E and F show signal-to-background values for excitation wavelength 1 and excitation wavelength 2, respectively, across all exposure times. Right-hand panels display a zoomed y-axis to better visualize the range at the critical threshold. Fura-10 and fura-8 reached the signal-to-background ratio of two (dotted line, Figs. 2E, F) at very short exposures (12/30 ms for Ex. 1 and 15/25 ms for Ex. 2), fura-2 at intermediate exposures (40 ms for Ex. 1 and 140 ms for Ex. 2), and fura-PE3 and fura-red only at longer exposures (150/160 ms for Ex. 1 and 300/300 for Ex. 2).

In summary, these measurements define optimized illumination times (as short as possible for comparable analysis quality) for each indicator as summarized in Table 3.

2.2. *Fura-10 as the calcium indicator of choice for long-term measurements and to preserve NK cell cytotoxicity*

To assess the suitability of the five different Ca^{2+} indicators for measurements in NK cells, we first monitored indicator fluorescence in NK cells over 12 h to rule out photobleaching, which could bias the analysis (Fig. 3A). The indicators behave differently and can be divided into three groups. Fura-PE3 and fura-red were relatively dim, and their fluorescence slowly increased during the experiments. This increase may be due to slower esterase cleavage, which could be problematic for a ratiometric indicator considering that not-cleaved indicators remain fluorescent and could compromise Ca^{2+} measurements. In addition, their dim signals are obviously problematic, as they complicate the analysis during tracking of the cells. Fura-2 and fura-8 both showed a fluorescence decrease over time which may be due to bleaching/leaking but was not investigated further. Fura-10 fluorescence, on the other hand, showed by far the brightest signal and was very stable over 12 h (Fig. 3A).

Next, we analyzed whether the indicators or their breakdown products after ester loading exhibit toxicity to NK cells without illuminating the indicators. We stained NK cells with the different fura-AM indicators and assessed NK cell functionality in a real-time population cytotoxicity assay compared to untreated controls. Additional control conditions were included, such as a DMSO control to exclude any effects of the dissolvent, and a BAPTA-AM-treated condition, since fura indicators are derived from this Ca^{2+} chelator [1]. None of the indicators measurably affected NK cytotoxicity, as shown by the cytotoxicity assay over four hours (Figs. 3B, C). Thus, we conclude that the indicators or their breakdown products are not toxic to NK cell functionality involved in cytotoxic processes over 4 h. Considering that NK cell's ability to eliminate target cells is not affected, it can be assumed that steps which are directly linked to cytotoxicity are not affected by the indicators. We excluded fura-PE3 from further testing as it performed worse than the other four indicators considering dynamic range, signal-to-noise ratio and brightness.

To determine which Ca^{2+} indicator is best suited for Ca^{2+} measurements while preserving NK cytotoxicity, we analyzed the effects of the different indicators on NK cytotoxicity against target cells in a microscopy-based set-up. We measured the indicator fluorescence in NK cells and the pCasper fluorescence in target cells to determine the time point and mode of cell death.

Using the FRET-based apoptosis reporter pCasper, we can classify target cell death induced by NK cells based on fluorescence changes [44]. Vital cells show signals for both GFP and FRET. Upon apoptosis, the reporter is cleaved resulting in disruption of FRET and a shift in fluorescence intensities: GFP fluorescence intensifies while FRET fluorescence decreases. Upon necrosis, due to disruption of the membrane integrity, the reporter is diluted, resulting in an overall loss of fluorescence in the cells.

Whether or not indicators influence NK cell cytotoxicity was solely determined by the resulting target cell death. For clarity, only the fluorescence of pCasper in the target cells is shown in representative microscopy images and not the fura signals in NK cells (Fig. 3D). For

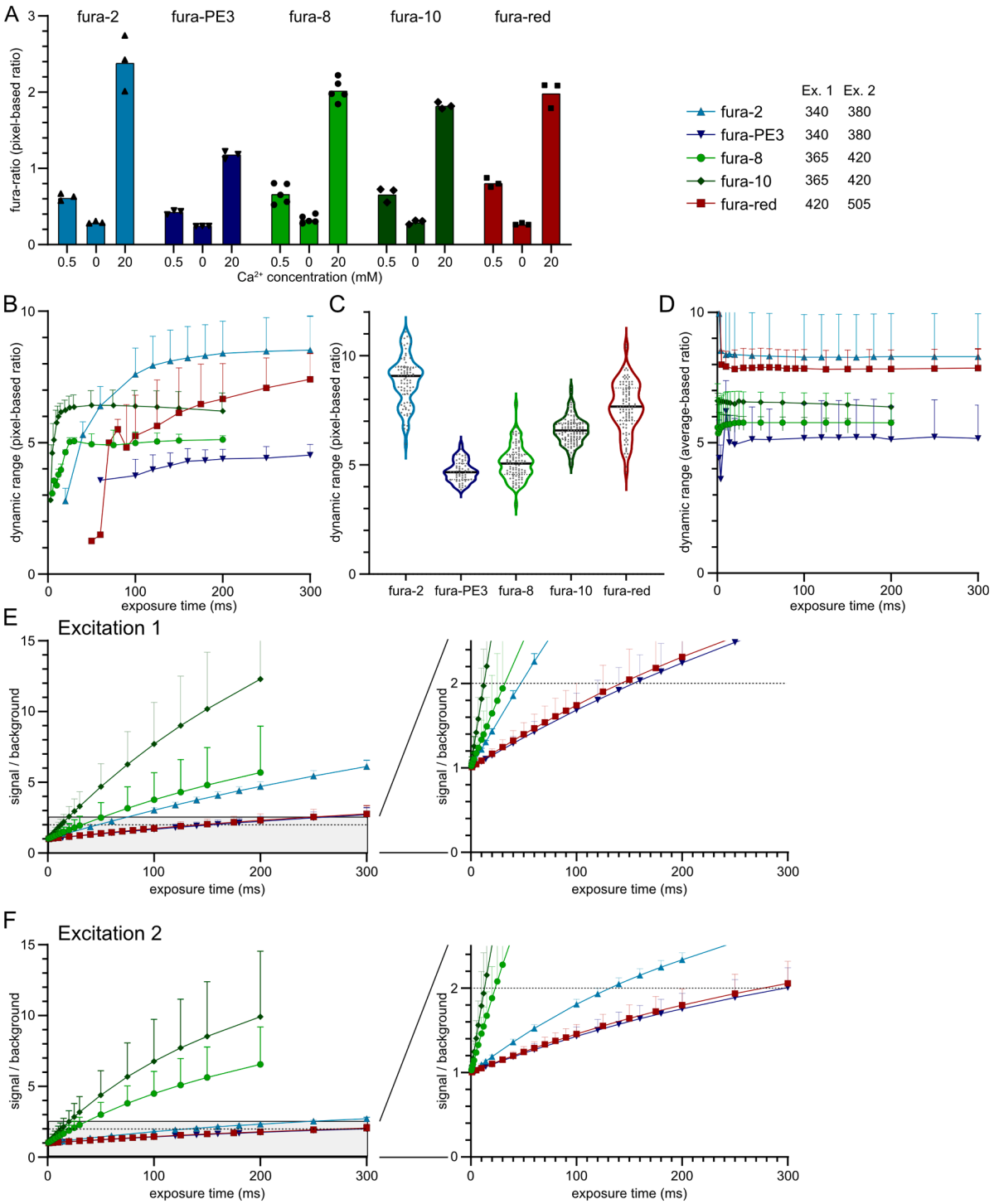

Fig. 2. Determination of optimal exposure times for Ca^{2+} imaging in primary NK cells. (A) Pixel-based calculated fura ratios of each indicator at 0.5 mM Ca^{2+}, 0 mM Ca^{2+} (1 mM EGTA, 1 μM thapsigargin and 4 μM ionomycin), and 20 mM Ca^{2+} (1 μM thapsigargin and 4 μM ionomycin). Exposure time was 200 ms for fura-8 and fura-10, 300 ms for fura-2, fura-PE3 and fura-red. Bars represent means; points indicate individual experiments ($n = 3–5$). (B) Dynamic range of indicators calculated from indicator-loaded primary NK cells using the pixel-based method at different exposure times. Data represent mean ± SD ($n = 3–5$ experiments). Since exposure time ratios were optimized to have comparable fura ratios under resting conditions and are thus different for each indicator (compare Table 2 and Fig. 2B), the dynamic range was always plotted against the exposure time of the wavelength with the longer exposure of the respective indicator, while the ratio of both wavelengths was kept constant. For fura-2 and fura-PE3, this was excitation wavelength 1 (Ex. 1), whereas for fura-8, fura-10, and fura-red, it was excitation wavelength 2 (Ex. 2). In all cases, the exposure at the other wavelength was adjusted to maintain the fixed inter-wavelength exposure-time ratio described above (Table 2). (C) Violin plots showing the dynamic range analyzed from individual cells at maximal excitation settings (200 ms for fura-8 and fura-10; 300 ms for fura-2, fura-PE3 and fura-red). Black bars indicate median values; dashed lines indicate quartiles ($n = 114–308$ cells). (D) Dynamic range calculated using the average-based method at different exposure times. Data are mean ± SD ($n = 3–5$ experiments). (E, F) Signal-to-background ratio (SBR) for each indicator at different exposure times for both excitation wavelengths. Right panels are magnification of left panels. Data represent mean ± SD ($n = 3–6$ experiments). Optimal exposure times for excitation wavelength 1 (Excitation 1) were: fura-2, 60 ms; fura-PE3, 160 ms; fura-8, 50 ms; fura-10, 15 ms; fura-red, 150 ms. For excitation wavelength 2 (Excitation 2): fura-2, 140 ms; fura-PE3, 300 ms; fura-8, 25 ms; fura-10, 15 ms; fura-red, 300 ms.

Table 3
Excitation and emission settings for phototoxicity assay.

Indicator	Excitation Ch1 LED (intensity, exposure time) + filter	Excitation Ch2 LED (intensity, exposure time) + filter	Beam splitter	Emission filter
Fura-2	365 nm LED (80 %, 140 ms) + 340/30 nm filter	380 nm LED (30 %, 70 ms) + 387/11 nm filter	BS 409 nm	510/90 nm
Fura-8	365 nm LED (8 %, 12 ms) + 370/10 nm filter	420 nm LED (8 %, 40 ms), no additional filter	BS 458 nm	510/90 nm
Fura-10	365 nm LED (8 %, 4,5 ms) + 370/10 nm filter	420 nm LED (8 %, 15 ms), no additional filter	BS 458 nm	510/90 nm
Fura-red	420 nm LED (30 %, 35 ms) + 427/15 nm filter	505 nm LED (30 %, 175 ms) + 504/17 nm	BS 440 nm, 520 nm, 607 nm	464/18 nm, 542/18 nm, 639/30 nm
GFP	470 nm LED (5 %, 20 ms) + 470/40 nm		BS 495 nm	525/50 nm
RFP-FRET	470 nm LED (5 %, 50 ms) + 470/40 nm		BS 593 nm	630/75 nm

each indicator we compared NK cells with and without the respective indicator. There was no illumination to excite fura indicators in case fura dyes were not loaded into NK cells. Fura-2, which is the most widely used indicator, significantly decreased single NK cell cytotoxicity as can be seen from the lack of target cell death in the respective images (Fig. 3D). Compared to control, in which in this case 4 target cells out of 18 cells were killed by apoptosis (green circles) and 3 by necrosis (white circles), only 3 (apoptosis) and 1 (necrosis) out of 26 cells were killed if fura-2 was present in NK cells and excited by 340/380 nm (Fig. 3D). Overall target cell death was thus 7 (out of 18) vs 4 (out of 26) in this example. The statistics of NK cells from 5 blood donors strengthens the significance of this conclusion. Fura-8, fura-10 and fura-red were inert to NK cell cytotoxicity as they did not interfere with NK cytotoxicity, whereas fura-2 clearly showed a combined photo-chemo-toxic effect (Figs. 3D, E).

In summary, we conclude from the combination of all tests that fura-10 is best suited for the analysis of Ca^{2+} signals in primary human NK cells (Fig. 3F). It is very bright, does not bleach or leak and is inert regarding NK cytotoxicity against target cells. Fura-10′s dynamic range does not quite match that of fura-2 or fura-red, however, it is certainly well suited to analyze Ca^{2+} signals in NK cells during cytotoxic activity against cancer cells. All other indicators have some limitations, with fura-2 being toxic to NK cell function under our conditions when excited at 340 and 380 nm.

Since fura-10 is the preferred indicator, we examined the autofluorescence of NK cells using its two excitation wavelengths of 365 and 420 nm on the Celldiscoverer 7, the microscope to be used for combined Ca^{2+} and cytotoxicity measurements. At both wavelengths we did not observe any autofluorescence in NK cells (Supplementary Fig. 3). Details are given in the respective figure legend. We conclude that autofluorescence of NK cells at 365 or 420 nm does not compromise fura-10 signals.

2.3. Fura-10 is well suited to report Ca^{2+} signals in intact murine pancreatic islets

To further evaluate the applicability of fura-10, we tested the indicator in a complex *ex vivo* model system, murine pancreatic islets. This model was chosen because of its stress-sensitive cell preparation. Representative images of fura-10-stained murine pancreatic islets from C57BL/6 J mice are shown in Fig. 4A. Cytosolic Ca^{2+} dynamics were recorded in response to sequential stimulation with 0.5 mM glucose, 20 mM glucose, and 30 mM KCl (Fig. 4B). Comparable experiments using fura-2 in pancreatic islets measured using a plate reader were reported previously [50] with similar outcomes, supporting that fura-10 is suitable not only for NK cell analysis, but also for other complex systems such as intact pancreatic islets.

2.4. Using fura-10 to correlate Ca^{2+} signals and cytotoxicity of NK cells from healthy blood donors

Our main goal is to develop a method to measure Ca^{2+} in primary human NK cells over extended times at 37 °C in a multi-well assay while preserving their cytotoxicity. For this, we used a Celldiscoverer 7 microscope with the settings shown in Table 4, as it combines environmental control, high throughput measurements and good imaging quality. For accurate analysis of Ca^{2+} levels in the context of cytotoxicity, it is essential to discriminate fura fluorescence from the fluorescence of the pCasper-expressing target cell. Fig. 5A shows fluorescence images of fura-10 loaded NK and K562-pCasper target cells. The merged image (left) shows the distinct separation of the NK cells (white / pink / violet) and the K562-pCaper cells (yellow / orange). On the right side, all individual images and respective merged images for NK and target cells are displayed. Only a negligible K562-pCasper signal appears in the fura-10 excitation 2 channel and the merged image, but not in the excitation 1 channel or pixel-ratio image (Fig. 5A). Although fura-10 signals of the NK cells slightly bleed into the K562-pCasper fluorescence images, the signal in the NK cells remains dim compared to the K562-pCasper cells and does interfere with pCasper signals. This is crucial for accurate tracking of the target cells in an automated manner and for distinguishing between vital, apoptotic, and necrotic cells. Next, we investigated single fluorescence traces from NK cells during different interactions with their respective targets over time, showing an NK cell without contact (Figs. 5B-D), one NK cell killing its target by apoptosis (Figs. 5E-G), and one killing its target by necrosis (Figs. 5H-J) using the pCasper reporter.

When an NK cell does not form any contact with its target, fluorescence intensities of both fura-10 channels remain stable (Fig. 5B, Supplementary Fig. 4A) and there is no significant change in the fura-10 ratio over time (365 nm/420 nm) (Fig. 5C, Supplementary Fig. 4A). The respective target cells show a relatively constant ratio of the GFP/FRET fluorescence (Fig. 5D) indicative of a vital cell (yellow / orange cell). Preceding NK-induced target cell death by apoptosis in the next example, there is a shift of fluorescence in the NK cells during K562 cell contact (Fig. 5E), resulting in a corresponding fura-10 ratio change over time indicative of a Ca^{2+} signal (Fig. 5F). NK cells were usually quiescent before contact and returned to baseline after contact (Supplementary Fig. 4B). The K562-pCasper target cell in the example (Fig. 5E) undergoes apoptosis upon contact with the NK cell, as indicated by a shift in fluorescence intensity from orange to green in the representative images and reflected in the GFP/FRET ratio of the pCasper reporter over time (Fig. 5G). The last example shows that also preceding necrosis, indicated by complete fluorescence loss of the target cell, there is a shift in fluorescence intensities of the NK cell (Fig. 5H) and a corresponding fura-10 ratio change over time indicative of a Ca^{2+} signal (Fig. 5I). The progression of necrosis is further confirmed by the decline of the GFP and FRET signals (Fig. 5J).

While K562 cells are often used to analyze natural cytotoxicity of primary human NK cells, other cell lines are clinically more relevant. Therefore, we established similar assays for NK cells against cancer cell lines which are relevant for studying acute myeloic leukemia (AML) or diffuse large B-cell lymphoma (DLBCL), namely THP1 and OCI-AML2 for AML and TMD8 for DLBCL. Examples of Ca^{2+} measurements in NK cells are shown during apoptotic (Figs. 6A-C) or necrotic (Figs. 6D-F) cell death of THP1-pCasper cells, during apoptotic cell death of OCI-AML2-pCasper cells (Figs. 6G-I), or during apoptotic (Figs. 6J-L) or necrotic (Figs. 6M-O) cell death of TMD8-pCasper cells. To allow TMD8 killing by NK cells, rituximab (1 μg/ml rituximab, 10 mg/ml stock solution) was included in the experiment (see [51] for details). The fura-10 signal not only allows the measurement of ratio and corresponding Ca^{2+} signals while preserving NK cell cytotoxicity against target cells over hours, but

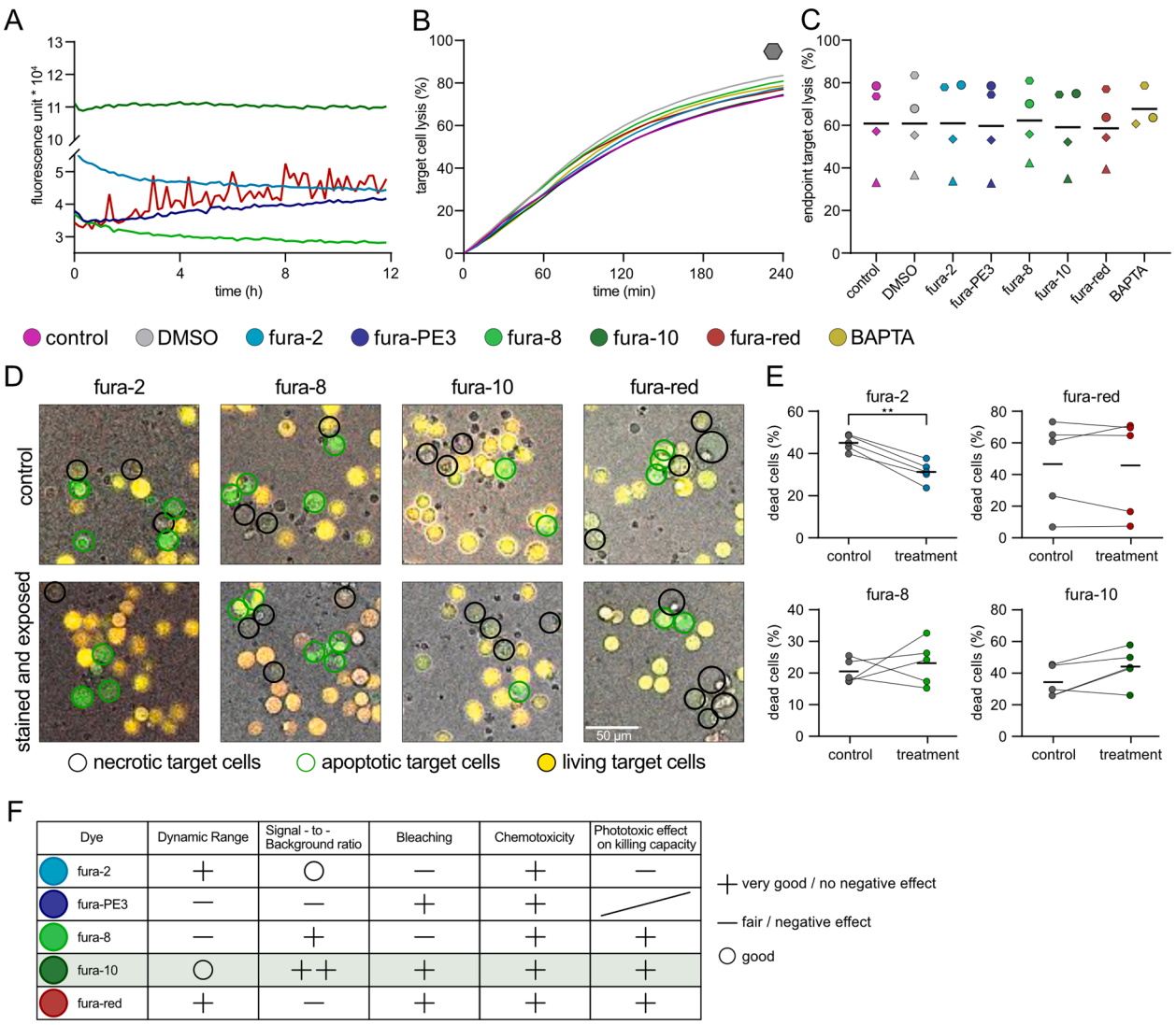

Dye	Dynamic Range	Signal - to - Background ratio	Bleaching	Chemotoxicity	Phototoxic effect on killing capacity
fura-2	+	○	–	+	–
fura-PE3	–	–	+	+	/
fura-8	–	+	–	+	+
fura-10	○	++	+	+	+
fura-red	+	–	+	+	+

Fig. 3. Long-term effects of fura indicators on NK cell cytotoxicity and fluorescence stability. (A) Fluorescence of fura-stained NK cells measured at the isosbestic point in a plate reader over 12 h at 37 °C (n = 3–4 experiments, mean ± SD). (B, C) Effect of different fura indicator loadings on NK cell-mediated lysis of calcein-loaded K562 target cells, measured by the real-time killing assay in a plate reader. DMSO and BAPTA were used as controls, and untreated cells were included as additional control. (B) Representative lysis kinetics over 4 h (of the experiment illustrated by hexagonal symbols from (C)). (C) Lysis rate after 4 h was not significantly different (n = 3–4 experiments, one-way ANOVA). Effector:target ratio, 3:1; NK cells were stimulated with IL-2. (D, E) NK cell killing capacity in long-term imaging experiments against E6.1 Jurkat-pCasper cells. (D) Representative images after 210 min for fura-stained and exposed versus control conditions (no fura). Black circles indicate necrotic E6.1 Jurkat-pCasper cells and green circles apoptotic ones. (E) Quantification of dead target cells after 210 min (n = 4–5 experiments; paired t-test). (F) Summary of the different tested parameters (dynamic range (Fig. 2B, C, D), signal-to-background ratio (Fig. 2E, F), bleaching (Fig. 3A), chemotoxicity (Fig. 3B, C) and the phototoxic effect on the killing capacity of NK cells (Fig. 3D, E)).

it can also be used to define immune synapse formation between NK cells and target cells. In addition, it defines the delay between initial contact/immune synapse formation and subsequent target cell death by apoptosis or necrosis.

2.5. *Using fura-10 to correlate Ca^{2+} signals and cytotoxicity of NK cells from patients with lymphoma and leukemia*

Up to now, only few studies have investigated NK cells at a single-cell level in the clinical context of disease. Therefore, we focused on NK cells from patients with acute myeloid leukemia (AML) or diffuse large B cell lymphoma (DLBCL) to analyze Ca^{2+} signals. We have succeeded in obtaining relatively pure (> 85 %) NK cell preparations from both types of patients. NK cells from those patients were loaded with fura-10 and their ratiometric signals were analyzed over time while simultaneously tracking K562-pCasper target cells (Fig. 7).

An AML-NK cell without contact is shown in Fig. 7A-C, and one that kills its target by apoptosis in Fig. 7D-F. Comparable to NK cells from blood donors, ratiometric fura-10 signals can be recorded over time while target cell death is simultaneously monitored. Identical experiments for DLBCL-NK cells are shown in Fig. 7G-L. Fig. 7G-I and 7J-L depict one example of an NK cell with no target contact and one with an NK cell killing a target cell by apoptosis, respectively.

In summary, these examples clearly show that fura-10 is ideally suited to quantify Ca^{2+} signals in NK cells from blood donors, AML, or DLBCL patients while simultaneously monitoring target cell states (vital, apoptotic, necrotic) over several hours without compromising NK cell cytotoxicity. In addition, fura-10 can be used to monitor immune synapse formation between NK and target cells, as Ca^{2+} signaling is an early event following NK cell receptor engagement. Finally, the ratiometric signals can be used to define the delay between initial contact of NK and target cells and apoptotic or necrotic target cell death caused by NK cell

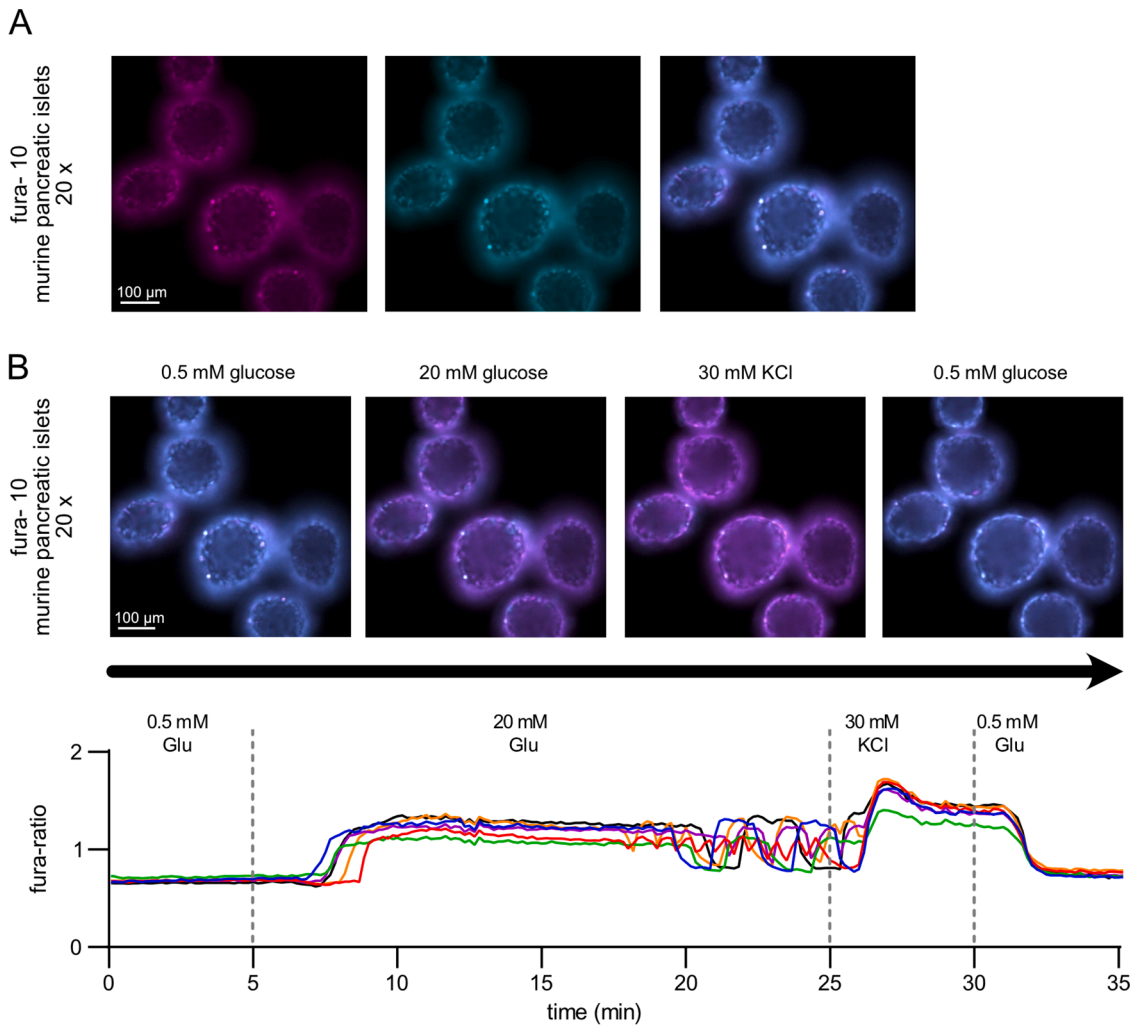

Fig. 4. Analysis of intracellular Ca^{2+} dynamics in murine pancreatic islets stained with fura-10. (A) Representative images of fura-10-loaded pancreatic islets from C57BL/6 J mice. Epifluorescence microscopy recordings after excitation at 360 nm (left) and 415 nm (middle), and the merged image of both channels are shown (right). (B) Cytosolic Ca^{2+} levels of C57BL/6 J pancreatic islets in 0.5 mM and in 20 mM glucose, followed by application and removal of 30 mM KCl concentration, monitored by fura-10 ratios (bottom). Scale bar = 100 µm. Below are the corresponding time lapse curves of the fura-10 ratios of 6 islets.

Table 4
Excitation and emission settings at the Celldiscoverer 7 to observe Ca^{2+} signaling with fura-10 as well as target cell death via the pCasper sensor.

Indicator		Excitation	Emission filter(s)
fura-10	Ex. 365 nm	365 nm LED, 7 %, 150 ms	514/26 nm
	Ex. 420 nm	420 nm LED, 12 %, 300 ms	514/26 nm
pCasper	Em. GFP	470 nm LED, 10 %, 120 ms	514/26 nm
	Em. FRET	470 nm LED, 10 %, 150 ms	592/18 nm

cytotoxicity.

3. Discussion

The findings of this study indicate that the synthetic Ca^{2+} indicator fura-10 is well suited for measuring and quantifying Ca^{2+} signals in primary human NK cells from blood donors and patients with lymphoma and leukemia, without compromising their cytotoxic functionality. Of the five tested ratiometric Ca^{2+} indicators fura-2, fura-PE3, fura-8, fura-10 and fura-red, fura-10 is the best candidate considering all properties tested. Most importantly, it is inert regarding NK cell functionality, it is the brightest indicator, it is the only one that does not bleach/leak over 12 h, it has a good dynamic range (almost as good as fura-2) and a very good signal-to-background ratio. In light of the aforementioned properties and the testing in human NK cells and murine pancreatic islets, both of which are very sensitive to external stress, fura-10 emerges as a very good option for Ca^{2+} measurements in other primary cells and cell lines. Given this, it is surprising that only two publications have reported the use of fura-10 [52,53] after it became available in 2020.

Since its initial introduction by Tsien and colleagues in 1985 [1], fura-2 has been used in at least 12.807 publications (PubMed search from 17.11.2025) and has been widely established in the Ca^{2+} field. However, introducing new or testing existing Ca^{2+}indicators is important for several reasons. One example highlighting the need for new indicators was shown by Robinson et al. (2023). They showed that the commonly used synthetic Ca^{2+} indicators fura-2 and fluo-4, and to a lesser extent rhod-2, impaired single-cell contractility of primary murine cardiomyocytes [3]. In contrast, they reported that genetically encoded Ca^{2+} indicators did not influence contractility. These findings may have broad implications as stated by the authors since Ca^{2+} measurements in cardiomyocytes are a common platform for cardiac toxicology testing [3]. In the present study, we report similar problems with fura-2 in primary human NK cells. We had already noticed previously that measurements of Ca^{2+} signals in the T cell line Jurkat E6.1 started to harm the cells after one hour of continuous fura-2 340/380 nm illumination applying a five second time interval. This evidence is circumstantial,

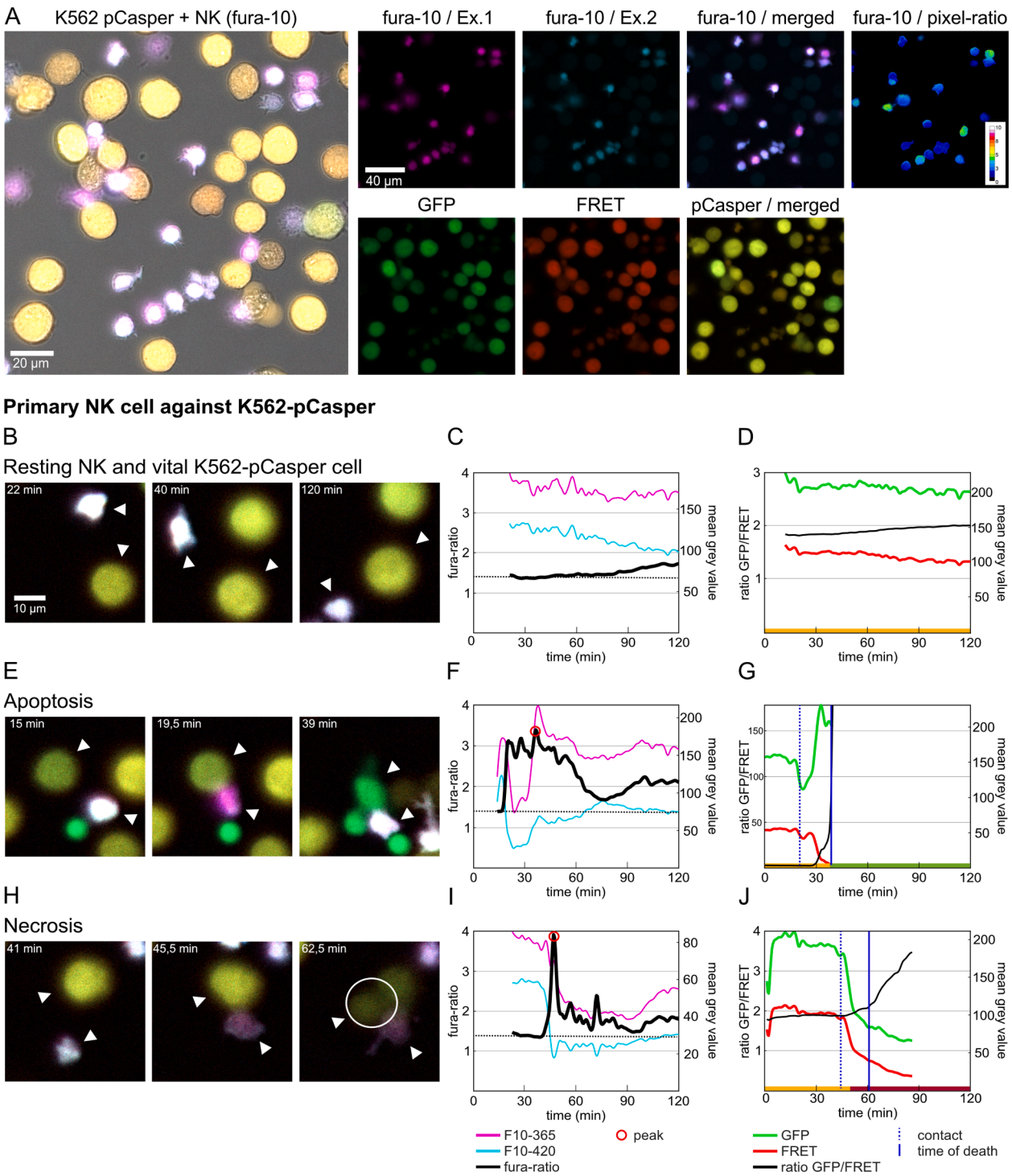

Fig. 5. Combined visualization of fura-10 Ca^{2+} signals in NK cells and target cell death with pCasper. (A) Co-incubation of primary NK cells loaded with fura-10 and K562-pCasper cells stably expressing the pCasper reporter. Left panel: Merged images of all channels (scale bar: 20 µm). NK cells appear white/pink and K562-pCasper cells yellow/orange indicating they are vital at the beginning of the experiment. Right upper and lower panel: NK and K562-pCasper cells shown in the respective fluorescence channels and their corresponding merged image. For NK cells, ratiometric Ca^{2+} imaging is shown as F365nm/F420nm pseudocolor map (scale bar: 40 µm). (B-H) Representative fura-10 signals in NK cells and pCasper signals in K562 cells with or without interaction (scale bar 10 µm). (B) Images of ratiometric fura-10 signals of a resting NK cell without K562-pCasper cell interactions. Scale bar 10 µm for this and all following images. (C) Fluorescence profile of fura-10 excited at 365 nm (pink) and at 420 nm (blue) and ratiometric fura-10 signals corresponding to a Ca^{2+} signal (black). (D) Fluorescence profile of a vital K562-pCasper cell showing the GFP signal (green), FRET signal (red), and the GFP/FRET ratio (black). (E) Images of ratiometric fura-10 signals of an NK cell before and during contact and after apoptotic cell death of its target K562-pCasper cell. (F, G) Fluorescence signals as shown in (C, D). (H) Images of the ratiometric fura-10 signal of an NK cell before and during contact and after necrotic cell death of its target K562-pCasper cell. (I, J) Fluorescence signals as shown in (C, D).

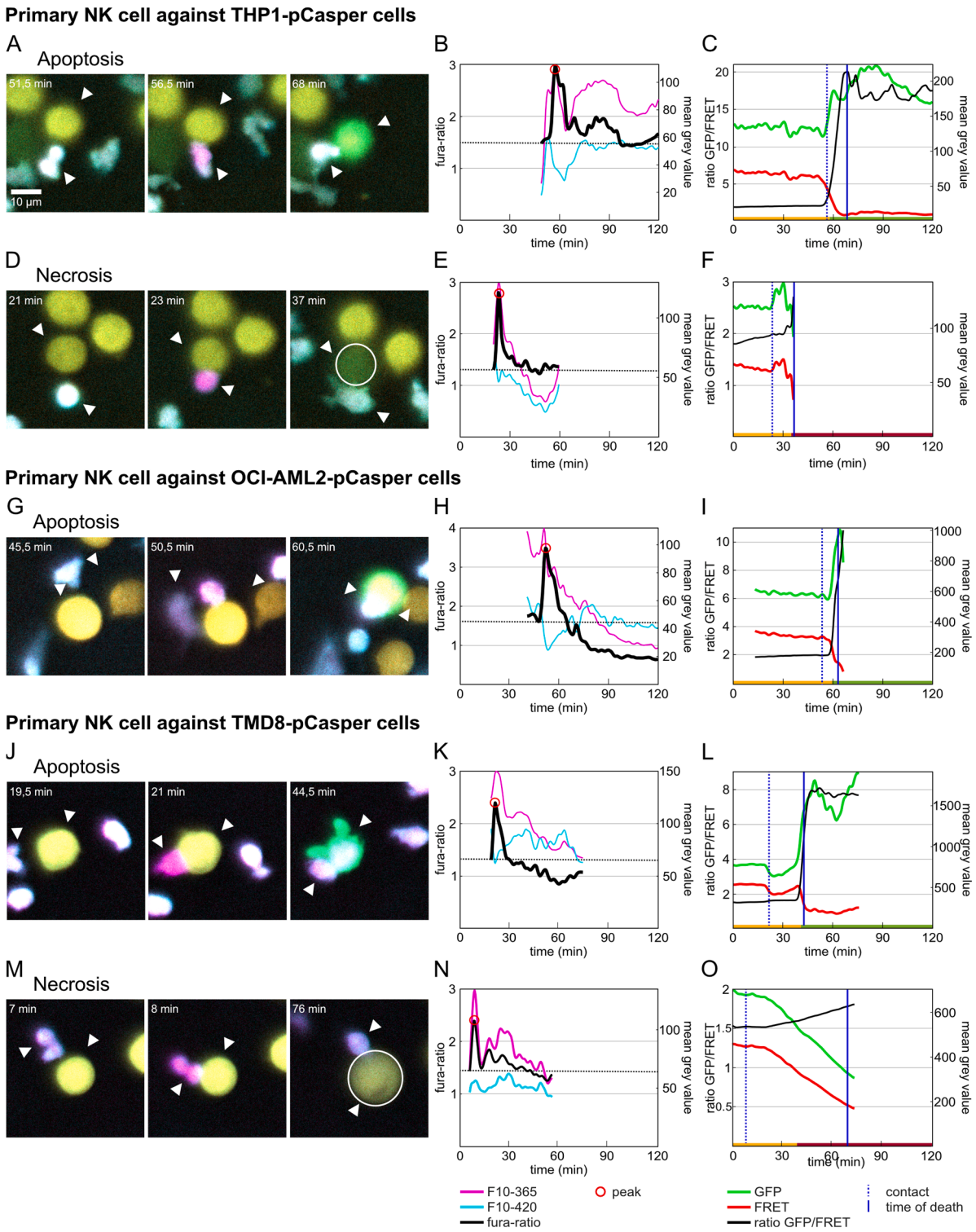

Fig. 6. Combined measurements of fura-10 Ca^{2+} signals in NK cells and cancer cell death of different pCasper cell lines relevant for acute myeloic leukemia (AML) or diffuse large B-cell lymphoma (DLBCL) research. (A-F) Representative Ca^{2+} signals of NK cells and pCasper signals in the AML cell line THP1-pCasper. (A) Merged image of ratiometric fura-10 signals of an NK cell before and during contact and after apoptotic cell death of its target THP1-pCasper cell. (B) Fluorescence profile of fura-10 excited at 365 nm (pink) and at 420 nm (blue) and ratiometric fura-10 signals corresponding to a Ca^{2+} signal (black). (C) Fluorescence profile of the apoptotic THP1-pCasper cell showing the GFP signal (green), FRET signal (red), and its GFP/FRET ratio (black). (D) Merged image of ratiometric fura-10 signals of an NK cell before and during contact and after necrotic cell death of its target THP1-pCasper cell. (E, F) Fluorescence signals as shown in (B, C). (G-I) shows fura-10 signals in an NK cell and apoptotic killing of an OCI-AML2-pCasper target cell (graphs similar as in A-C). (J-L) shows fura-10 signals in an NK cell and apoptotic killing of an TMD8-pCasper target cell (graphs similar as in A-C). Rituximab was included to mediate antibody-dependent cytotoxicity of NK cells against TMD8 cells. (M-O) shows fura-10 signals in an NK cell and necrotic killing of an TMD8-pCasper target cell (graphs similar as in D-F). Rituximab was included to mediate antibody-dependent cytotoxicity of NK cells against TMD8 cells. Scale bar 10 µm for all images.

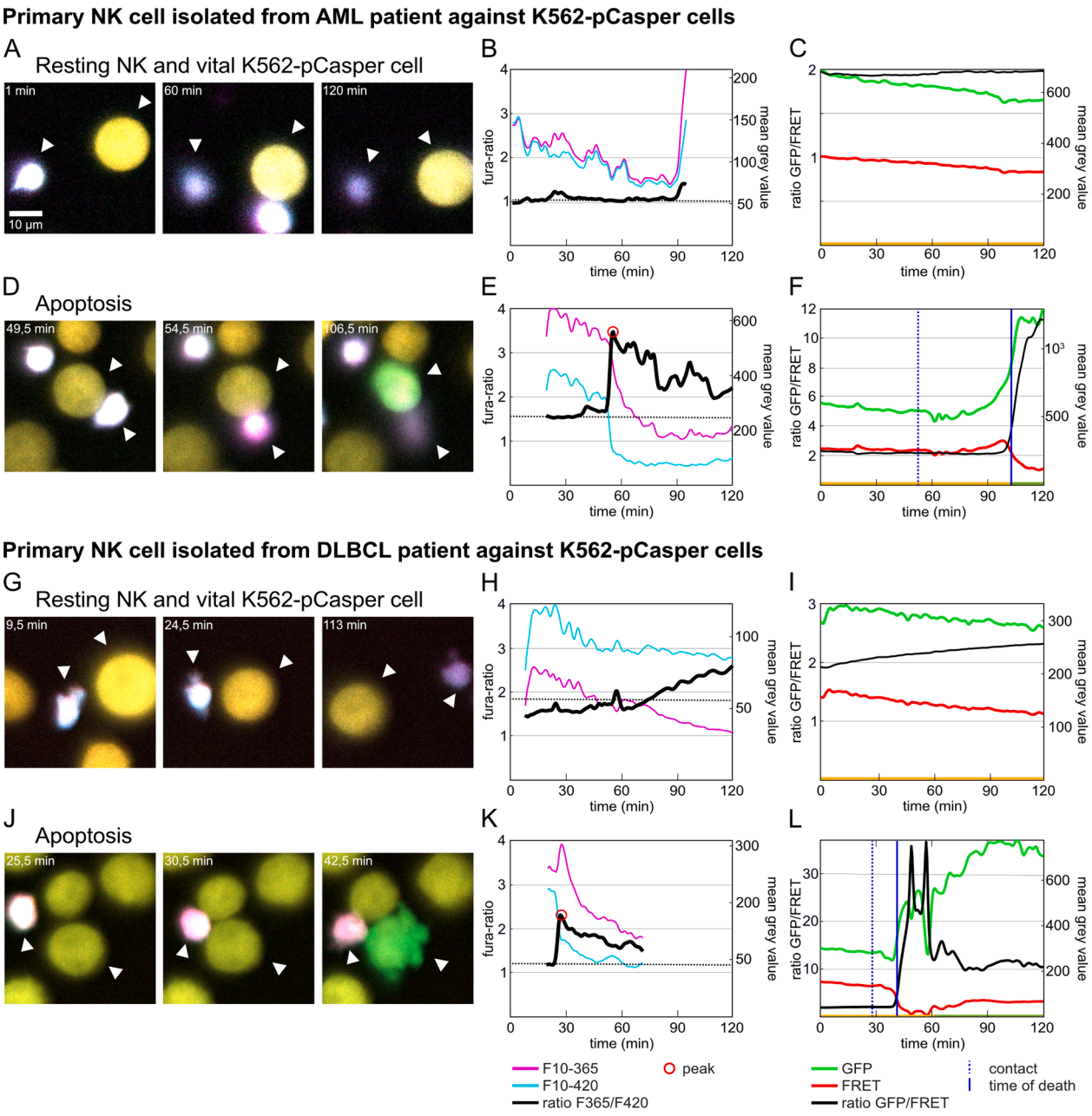

Fig. 7. Correlation of fura-10 Ca^{2+} signals in NK cells from patients with acute myeloic leukemia (AML) or diffuse large B-cell lymphoma (DLBCL) and K562 target cell death. (A-F) Representative fura-10 signals of NK cells isolated from AML patients. (A) Merged image of ratiometric fura-10 signals of an AML-NK cell without K562-pCasper cell interaction. (B) Fluorescence profile of fura-10 excited at 365 nm (pink) and at 420 nm (blue) and the ratiometric fura-10 signal (black). (C) Fluorescence profile of vital K562-pCasper cell showing the GFP signal (green), FRET signal (red), and its GFP/FRET ratio (black). (D) Merged image of ratiometric fura-10 signals of an AML-NK cell before and during contact and after apoptotic cell death of its target K562-pCasper cell. (E, F) Fluorescence signals as shown in (B, C). (G-L) same as (A-F), only that DLBCL-NK cells were used instead of AML-NK cells. Scale bar 10 µm for all images.

however combining the results in cardiomyocytes [3] and our data on primary human NK cells, fura-2 illumination at the optimal wavelength of 340/380 nm may be harmful to cells over extended periods of time. Our results do not point towards chemical toxicity of fura-2 or its fission products after de-esterification but rather to a combined photo-chemo-toxicity of fura-2.

The second reason for a likely decrease in fura-2 use in the future comes from a change in illumination sources which has occurred over the last ten years. For epifluorescence measurements the standard has changed to light-emitting diodes (LEDs) away from xenon or mercury arc lamps with a monochromator as discussed recently by Zhou *et al.* [6]. LEDs have many advantages compared to arc lamps including fast intensity regulation, fast electronic shuttering within milliseconds, and high stability [6,54]. Furthermore, their spectrum usually does not extend into the UV spectrum below 300 nm which is the case for arc lamps. If these very short wavelengths are not completely eliminated by filter systems, they may severely harm cells over extended times. This may even go unnoticed if only very little UV intensity below 300 nm is transmitted. Although 340/380 nm LEDs are now available [54] and ideal for fura-2 use, they are not routinely built into microscopes with LED illumination. Custom-made solutions are available but expensive.

Zhou et al. [6] compared a newly developed ratiometric Ca^{2+} indicator called isoCaRed-1Me to fura-2 and fura-red using the typically available LEDs in a commercial microscope. Excitation of isoCaRed-1Me

or fura-2 was carried out at 390 nm and 475 nm, which of course did not work for fura-2. However, isoCaRed-1Me was brighter than fura-red making it an interesting alternative red-shifted Ca^{2+} indicator.

While fura-2 was toxic for NK cells under the conditions used here, fura-red and fura-8 were not. However, they were rather dim and did not show stable fluorescence over four hours unlike fura-10. Fura-red has been shown to have a lower quantum yield than fura-2 (see [55] for review). While fura-8 bleached/leaked a bit over 12 h, it could have been also used for Ca^{2+} measurements in NK cells. However, since fura-10 is brighter than fura-8 and less prone to leakage it is, among the tested ones, the Ca^{2+} indicator of choice for primary human NK cells and potentially other primary cells.

The Ca^{2+} signals reported here with fura-10 at 37 °C in NK cells after target cell contact are transient, often only 30 min or less. There are sometimes few oscillations, but they fade quickly with no prominent Ca^{2+} plateau. We are aware of only one other report by Honda and Miyazaki [28] which reports human NK cell Ca^{2+} signals in response to contact with K562 or MOLT-4 target cells measured with fura-2 at room temperature. These Ca^{2+} signals look similar. Fura-10 allowed us to measure Ca^{2+} signals in natural killer (NK) cells from patients diagnosed with acute myeloid leukemia (AML) or diffuse large B-cell lymphoma (DLBCL). Preparing NK cells from AML patients is particularly challenging, often yielding low numbers. Fura-10 enables Ca^{2+} measurements over several hours in NK cells from AML patients during cytotoxicity against cancer cells. This is a prerequisite for understanding potential functional Ca^{2+} dependent impairments in these patients.

Interestingly, only very little Ca^{2+} influx is sufficient to maintain cytotoxic NK cell activity and NK cells operate best at a rather low Ca^{2+} optimum [12,29,30]. We showed that a block of CRAC/Orai1 channels in CTL enhanced cytotoxicity [30], and likewise, Olivas-Aguirre et al. found that a block of KCa3.1 in NK cells had the same effect as it reduces the driving force for Ca^{2+} entry [29]. However, only little data exists on the source of Ca^{2+} to raise intracellular Ca^{2+} signals in NK cells. PLC-γ2 is essential for NK cytotoxicity [56]. Influx across the plasma membrane is likely required for NK cytotoxicity and genetic evidence shows that it may be largely mediated by CRAC/Orai1 channels [13], a view that has been confirmed by metabolic screening in cytotoxic T lymphocytes [57]. However, the role of TRP channels for Ca^{2+} influx has also been reported in NK cells. These include TRPC3 [16], TRPM2 [33], TRPM3 [20,21,32], and TRPM7 [31]. In addition, it is not clear what role Ca^{2+} release from internal stores plays for NK cell function compared to Ca^{2+} influx across the plasma membrane.

We believe it is important to find out which receptors induce which Ca^{2+} signals in NK cells. Only few data have been published. Ganesan and Höglund showed that NK1.1 and MHC class 1 molecules induce additive Ca^{2+} signals in murine NK cells [15], whereas Ly49A dampens Ca^{2+} signals in murine NK cells induced by NKp46 or NK1.1 [14]. In addition, Cassatella et al. and Theorell and Bryceson showed that crosslinking stimulation of CD16 induces Ca^{2+} signals in primary human NK cells [24,35]. This is important as CD16 is an important receptor involved in rituximab therapy of lymphoma [58,59].

In light of the pivotal role that Ca^{2+} signals play in the signaling processes of NK cells, it is imperative to acknowledge the necessity for a more comprehensive and detailed understanding of Ca^{2+} dynamics. This enhanced knowledge base is potentially also important for improving the efficacy of NK cell-based therapeutic interventions. Fura-10 is a very good tool to achieve this as it preserves NK cytotoxicity against cancer cells and allows quantification of Ca^{2+} signals in long-term experiments.

4. Materials and methods

4.1. Ethical approval

Experiments with mononuclear blood cells and patient samples are approved by the local ethics committee (reference 84/15, 33/18 and 272/22). The local blood bank of the Institute of Clinical Hemostaseology and Transfusion Medicine at Saarland University Medical Centre provided leucocyte reduction system (LRS) chambers, a byproduct of platelet collection from healthy blood donors. All blood donors and patients provided informed, written consent to use their blood for research purposes.

Experiments with murine cells are approved by the local governmental animal protection committee (LAV Saarland and Animal Welfare Officer Saarland University). Islets isolation has been announced according to local regulations of Saarland University and Saarland Authorities (§4 Tierschutzgesetz / killing of animals).

4.2. Preparation and maintenance of natural killer (NK) cells from blood donors

Human peripheral blood mononuclear cells (PBMCs) were obtained from healthy donors after routine platelet apheresis using leukocyte reduction chambers (LRS) of Trima Accel devices (Institute of Clinical Haematology and Transfusion Medicine, Homburg, Germany). PBMCs were isolated by density gradient centrifugation with Lymphocyte Separation Medium 1077 (PromoCell, Germany) as described previously [60]. Primary NK cells were isolated from PBMCs using the NK Cell Isolation Kit (Miltenyi Biotec, Germany) according to the manufacturer's instructions using an AutoMACS system (Miltenyi Biotec, Germany). NK cells were cultured at 2×10^6 to 3×10^6 cells/ml in AIM-V medium (Gibco AIMV, Thermo Fisher Scientific, USA) supplemented with 10 % fetal bovine serum (FBS, Invitrogen; Thermo Fisher Scientific USA). On the day of isolation, cells were stimulated with 100 U/ml recombinant human IL-2 (human IL-2 recombinant protein; Miltenyi Biotec, Germany) and used for experiments 2–6 days after isolation.

4.3. Preparation and maintenance of natural killer (NK) cells from patients

PBMCs from DLBCL patients were isolated from EDTA blood samples by density gradient centrifugation using Lymphocyte Separation Medium 1077 (PromoCell, Germany) as described previously [51]. NK cells were purified using antibody-coupled magnetic beads from Miltenyi Biotec according to the manufacturer's specifications. Monocytes, granulocytes and remaining erythrocytes were depleted from freshly isolated PBMC using CD14, CD15 and CD235A MicroBeads and LD columns (Miltenyi Biotec, Germany). T cells were then depleted from the negative population using CD3 MicroBeads. NK cells were isolated from the CD3-negative population using CD56 MicroBeads (Miltenyi Biotec, Germany). The purity of the isolated NK was confirmed by flow cytometry (for use in cytotoxicity assay purity >85 %). Isolated cells were cultured in AIMV + 10 % FBS at 37 °C and 5 % CO_2 overnight [51].

PBMCs from AML patients were isolated from EDTA blood samples by density gradient centrifugation as described previously [51]. One important step was optimized for AML samples due to the high number of leukemic blasts in the blood. Instead of a one-step density gradient, a two-step density gradient was performed with Lympholyte-Poly (1.113 g/ml) (Biozol, Germany) and Lymphocyte Separation Medium 1077 (PromoCell, Germany). All following steps remained unchanged. T cells were then depleted from the negative population using CD3 MicroBeads. NK cells were isolated from the CD3-negative population using CD56 MicroBeads. The purity of the isolated NK was confirmed by flow cytometry (for use in cytotoxicity assay purity >85 %).

4.4. Cell lines

The following cell lines were used: E6.1 Jurkat cells (ATCC, TIB-152™), K562 cells (CCL-243), TMD8 (Cellosaurus, TMD8 (CVCL_A442), kindly provided by Lorenz Trümper, Göttingen), OCI-AML2 (DSMZ, ACC99, kindly provided by Evelyn Ullrich, Frankfurt) and THP1 (TIB-202™).

E6.1 Jurkat-pCasper cells were generated as described in [44]. The

Luc2-pCasper cells (K562-Luc2-pCasper, OCI-AML2-Luc2-pCasper and THP1-Luc2-pCasper cells) were generated by lentiviral transduction as recently described [51].

TMD8-pCasper (MC pC clone 4_23) and K562-pCasper (SB-pCasper clone 43) were generated using the Sleeping Beauty system. SB100XmRNA was in vitro transcribed using the plasmid IVTRup-SB100x as described before [61–63]. TMD8 cells were transfected with pCasper Minicircle (pCasper coding sequence from Evrogen (#FP971), EF1A promoter, ITR (VectorBuilder)) generated by PlasmidFactory GmbH. K562 cells were transfected with a Sleeping Beauty Transposon Gene Expression Vector (SBTGEV-pCasper, VectorBuilder) containing the same EF1A promoter, ITR and pCasper coding sequence as for the Minicircle (SBTGEV-pCasper, VectorBuilder). SB100X-mRNA and pCasper Minicircle or SBTGEV-pCasper (ratio 5:1) were nucleofected using Nucleofector 4D technology (SF kit, pulse code EW-113 for TMD8 and FF-120 for K562). TMD8 populations were sorted (Cell Sorter SH800S (Sony)) followed by single cell cloning, and clone 4.23 was used. K562 populations were single cell cloned. K562-pCasper (SB-pCasper clone 43) were used for experiments with DLBCL patient NK cells (Fig. 7), and K562-Luc2-pCasper cells were used for experiments with NK cells from blood donors and for experiments with AML patient NK cells (Figs. 5, 7).

All cell lines were cultured at 37 °C in a humidified incubator with 5 % CO_2 in RPMI-1640 medium (ThermoFisher Scientific, USA) supplemented with 10 % FBS 1 % penicillin/streptomycin (P/S; Sigma-Aldrich). For E6.1 Jurkat-pCasper cells, 0.8 mg/ml G418 (ThermoFisher Scientific, USA) was added as a selection marker for stable pCasper expression [44]. THP1 medium additionally contained 1 % NEAA, 1 % Sodium Pyruvate and 50 µM ß-Mercaptoethanol. OCI-AML2-Luc2-pC were cultured in MEM-alpha (ThermoFisher Scientific, USA) containing 20 % FBS and 1 % P/S.

4.5. Chemicals and reagents

Stock solutions of fura-2 AM (molecular probes; Thermo Fisher Scientific, USA), fura-PE3 AM (Santa Cruz, USA), fura-8 AM and fura-10 AM (both from biomol, Germany, manufacturer AAT bioquest, USA), and fura-red AM (Thermo Fisher Scientific, USA) were prepared in DMSO at 1 mM stock concentration, aliquoted, and stored at –20 °C until use. Fura-2, fura-8 and fura-10 were used at 1 µM, fura-PE3 and fura-red at 2 µM. The following chemicals were used: thapsigargin (Thermo Fisher Scientific, USA), ionomycin (Merck, Germany), rituximab (provided by the local pharmacy; Hexal AG, Germany). All other chemicals not explicitly mentioned were from Merck (Germany), highest grade. Calcium buffer compositions were as follows: 0 mM Ca^{2+} (EGTA buffer): 145 mM NaCl, 4 mM KCl, 10 mM glucose, 10 mM HEPES, 2 mM $MgCl_2$, and 1 mM EGTA, pH 7.4. 0.5 mM Ca^{2+}: 145 mM NaCl, 4 mM KCl, 10 mM glucose, 5 mM HEPES, 2 mM $MgCl_2$, and 0.5 mM $CaCl_2$, pH 7.4. 20 mM Ca^{2+}: 145 mM NaCl, 4 mM KCl, 10 mM glucose, 5 mM HEPES, 2 mM $MgCl_2$, and 20 mM $CaCl_2$, pH 7.4.

4.6. Flow cytometry

Flow cytometry was performed using a FACSVerse (BD Bioscience, Germany) and the FlowJo v10.8.1 data analysis software (BD, USA) to analyze PBMC and PBMC subpopulations. As described before [60], NK cells and other PBMC subtypes like T cells, B cells and monocytes were identified by a combination of physical parameters (SSC-A; FSC-A, FSC—H) and surface staining with fluorochrome-conjugated mAbs (anti-CD3-PerCP (SK7), anti-CD16-PE (B73.1), anti-CD14-PE-Cy7 (MSE2), anti-CD56-APC (HCD56), anti-CD8-FITC (SK1), anti-CD4-BV421 (SK3), anti-CD45-BV510 (HI30) and anti-CD19-BV421 (HIB19). All antibodies were from BioLegend (Revvity, USA) and were incubated for 20 min at RT. The same panel was used to verify the purity of NK cells.

4.7. Spectral analysis with a plate reader

Spectral measurements were performed in a CLARIOstar plate reader (BMG Labtech, Germany) at 37 °C. Fura-loaded cells and unstained control cells were settled in a black 96 well plate in a density of 250.000 cells/well. Two different conditions were executed: 0 mM Ca^{2+} condition: 1 mM EGTA, 1 µM thapsigargin and 4 µM ionomycin; 20 mM Ca^{2+}: 20 mM $CaCl_2$, 1 µM thapsigargin and 4 µM ionomycin. Excitation and emission scans were acquired at 1 nm increments.

Fluorescence values from unstained cells in the corresponding Ca^{2+} buffer were subtracted from indicator-loaded samples. For each experiment, technical replicates of 1–3 wells were averaged and normalized to the maximum fluorescence.

4.8. Ca^{2+} imaging with the cell observer

Live-cell imaging was performed at 37 °C using a Zeiss Cell Observer microscope equipped with a Colibri LED (Zeiss, Germany) light source, Evolve EMCCD camera (Photometrics, USA) and appropriate excitation/emission filter sets (Table 2).

Glass coverslips (25 mm diameter, Orsa tec, Germany) were coated with 50 µl of 0.1 mg/ml poly-L-ornithine for 30 min, and 1×10^5 NK cells in 5 µl AIM-V were seeded and allowed to adhere for 30 min. For calibration, cells were sequentially perfused with 0.5 mM Ca^{2+} buffer, 0 mM Ca^{2+}buffer (with 1 mM EGTA, 1 µM thapsigargin and 4 µM ionomycin) for 5 min, or 20 mM Ca^{2+}buffer (also with 1 µM thapsigargin and 4 µM ionomycin) for 1 min. Imaging was performed at each step with the indicated exposure times.

4.9. Analysis of Ca^{2+} imaging data

The dynamic range was calculated using two different analysis approaches. The pixel-based ratio was calculated using the ImageJ Plugin Ratio NaN. From these images, the mean fura ratio per cell was determined at 0 mM Ca^{2+} (1 mM EGTA, thapsigargin and ionomycin) and at 20 mM Ca^{2+}. Then the dynamic ranges of the indicators were calculated. The second approach, the average-based ratio, was calculated by the mean fluorescence intensity per channel for each cell. These values were used to derive the fura ratio per cell, followed by averaging all cells for each condition. The dynamic range was then determined from these mean values, yielding one value per experiment.

For both pixel-based and average-based methods, background correction was performed using ROI-based subtraction. Two background ROIs were manually defined, and their mean fluorescence intensity was calculated and used as background value. In the pixel-based analysis, this background value was set in the Ratio NaN plugin, while in the fluorescence-based analysis it was manually subtracted from the measured intensities.

To create ratiometric images the ImageJ plugin Ratio NaN was used. The clipping value was set to the background plus twice the standard deviation of the background ROIs.

Ca^{2+} analysis of data acquired with the Celldiscoverer 7 was performed with a customized MATLAB script, using fluorescence-based fura ratio calculation.

4.10. Calcein-based real-time killing assay

Real-time killing assays of populations were performed as previously described [64] using a CLARIOstar plate reader (BMG Labtech, Germany). Briefly, K562 target cells were loaded with 500 nM Calcein-AM in AIM-V medium containing 10 mM HEPES for 20 min at room temperature, washed once, and seeded into black clear-bottom 96-well plates (VWR, USA) at 2.5×10^4 cells/well. NK cells were loaded with fura indicators or control compounds for 30 min, washed twice, and resuspended in AIM-V medium. The effector to target ratio was 3:1. Untreated NK cells were treated in the same way. Target cell lysis was

measured via fluorescence reduction every 10 min for 4 h at 37 °C in bottom-reading mode in the CLARIOstar plate reader. Excitation was performed at 482/16 nm and emission at 530/40. Fluorescence measurement was done in spiral mode and bottom reading. Data analysis was performed as in [64].

4.11. Bleaching analysis with the plate reader

Photobleaching was assessed at 37 °C using the CLARIOstar plate reader. For each fura indicator, the following settings were used: fura-2 and fura-PE3 (excitation 360/20 nm, emission 500/20 nm), fura-8 and fura-10 (excitation 380/20 nm, emission 500/20 nm), fura-red (excitation 450/20 nm, emission 660/20 nm). 250.000 cells per well were measured in a spiral scanning pattern every 10 min for 710 min. Data from 2 to 3 wells per indicator were averaged.

4.12. Phototoxicity assay with the cell observer

Phototoxic effects were tested in a co-culture of NK cells and E6.1 Jurkat-pCasper target cells at an effector to target (E:T) ratio of 3:1 in a 96-well plate. NK cells were labelled with the respective fura indicators and imaged at the optimal exposure times defined as signal-to-background-value over 2, as shown in Table 3. During the observation period of 3.5 h, ratiometric fura imaging was performed every 1 min, combined with pCasper fluorescence and transmitted light acquisition every 30 min to monitor NK cell cytotoxic activity. As a control, unstained and non-exposed NK cells of the same donors were imaged. The NK cell mediated killing in control wells was measured by pCasper fluorescence every 30 min. Measurement was done at 37 °C under 5 % CO_2.

4.13. Simultaneous Ca^{2+} and cancer cell death imaging with fura-10 and pCasper using a celldiscoverer 7

Live-cell Ca^{2+} imaging was performed at 37 °C with 5 % CO_2 on the Celldiscoverer 7 (Zeiss, Germany) imaging platform using black flat bottom 96 or 384 well plates (Revvity, USA). NK cells from blood donors as well as patient-derived NK cells were prepared and stained as described above. As target cells, K562-pCasper, OCI-AML2-pCasper, THP1-pCasper and TMD8-pCasper were used. 10.000 target cells were seeded in 384 well plates and incubated during measurement with NK cells in an effector-to-target (E:T) ratio of 1.5:1. Exposure times, excitation and emission filters used for fura-10 and pCasper are summarized in Table 4.

4.14. Analysis of cytosolic Ca^{2+} signaling in murine pancreatic islets with fura-10

C57BL/6J mice were used to obtain pancreatic islets used for Ca^{2+} imaging experiments. All animals were housed in the animal facility of the Center for Integrative Physiology and Molecular Medicine (CIPMM) at Saarland University, free from murine pathogens. All procedures were conducted in compliance with the ethical guidelines and approved by the local ethics committee.

Krebs-Henseleit buffer of the following composition was used for experiments with pancreatic islets: BSA 0.2 % (0.1 % for measurements), $CaCl_2$ 2.5 mM, Glucose 10 mM (varied in experiments), HEPES 5 mM, KCl 4.8 mM, $MgCl_2$ 1.2 mM, Na-bicarbonate 24 mM, NaCl 120 mM, P/S 1 % (no P/S for measurements).

Pancreatic islets were isolated from C57BL/6 J mice by enzymatic digestion. Collagenase P (0.63 mg/ml; Roche Diagnostics GmbH, Ref: 11,213,865,001) in Krebs-Henseleit buffer was used to perfuse the pancreas via the pancreatic duct. The pancreas was removed, incubated in a water bath for 20 min at 37 °C before the tissue was shaken manually and washed with Krebs-Henseleit buffer and centrifuged thrice for 5 min at 140 x g. Islets were further purified manually from exocrine tissue with assistance of a stereo microscope (Stemi 305, Zeiss) and cultured overnight in RPMI 1640 medium (Gibco, Thermo Fisher Scientific, USA) supplemented with 10 % FBS (Gibco, Thermo Fisher Scientific, USA) and 1 % penicillin/streptomycin (Sigma Aldrich, Germany) at 37 °C and 5 % CO_2 until used for measurements.

Cytosolic Ca^{2+} levels of murine pancreatic islets were investigated by using the ratiometric indicator fura-10. Islets were loaded with fura-10 AM (5 μM) for 2 h at 37 °C and 5 % CO_2. Afterwards they were washed twice and starved in 0.5 mM glucose Krebs-Henseleit buffer before they were placed by hand under the stereo microscope in a custom build microscopy chamber. Cellular Ca^{2+} levels were assessed with an Axio Observer 7 inverted epifluorescence microscope (Zeiss) at continuous perfusion of the pancreatic islets at 1 ml/min flow speed with low (0.5 mM) and high (20 mM) glucose concentration, while 30 mM KCl served as a depolarizing control.

4.15. Statistical analysis

Data are presented as mean ± SD, with n indicating the number of cells or experiments as specified in figure legends. Statistical analyses were performed with Prism 10 (GraphPad Software Inc., USA). Shapiro-Wilk test was used for normality test. Paired student's *t*-tests were used for two-group comparisons, RM one-way ANOVA was done for multiple comparisons. * $p < 0.05$, ** $p < 0.01$, or *** $p < 0.001$ were considered statistically significant.

Funding sources

This project was supported by grants from the Wilhelm-Sander-Stiftung (2023.100.1), the Dr. Rolf M. Schwiete Stiftung (2023–028) (both to MHoth and LT), and the BMBF (031L0252, to MHoth). EU acknowledges the Stiftung Deutsche Krebshilfe (German Cancer Aid; "CAR FACTORY" #70,115,200) and the Deutsche Forschungsgemeinschaft (SFB 1292, TP 12, Project-ID 318,346,496). In addition, we acknowledge large equipment grants: INST 256/555–1 FUGG for a screening microscope with confocal function (Celldiscoverer 7), INST 256/423–1 FUGG for a flow cytometer (BD Biosense, FACS Verse). Generation of minicircles was supported by the IRTG/SFB1027 mini-proposal 2024 to JV.

Declaration of generative AI in scientific writing

In order to improve the grammar of individual sentences, ChatGPT (o1-preview), OpenAI or DeepL/Pro were used. After using these tools, the authors reviewed and edited the sentences as needed, and they take full responsibility for the content of the published article.

CRediT authorship contribution statement

Lea Kaschek: Writing – review & editing, Writing – original draft, Visualization, Validation, Supervision, Software, Project administration, Methodology, Investigation, Formal analysis, Data curation, Conceptualization. **Joanne Vialle:** Writing – review & editing, Writing – original draft, Visualization, Validation, Software, Methodology, Investigation, Formal analysis, Data curation, Conceptualization. **Gebhard Stopper:** Writing – review & editing, Writing – original draft, Validation, Software, Methodology, Investigation, Conceptualization. **Markus D.A. Hoffmann:** Writing – review & editing, Visualization, Validation, Methodology, Investigation, Formal analysis, Data curation, Conceptualization. **Sylvia Zöphel:** Writing – review & editing, Validation, Methodology, Investigation, Formal analysis, Data curation. **Johanna Jansky:** Writing – review & editing, Validation, Methodology, Investigation, Formal analysis. **Nadja Küchler:** Writing – review & editing, Validation, Methodology, Investigation, Formal analysis. **Gertrud Schäfer:** Writing – review & editing, Validation, Methodology, Investigation, Formal analysis. **Alina Moter:** Writing – review & editing,

Validation, Methodology, Investigation, Formal analysis. **Philipp Wendel:** Writing – review & editing, Validation, Methodology, Investigation, Formal analysis. **Frank Neumann:** Writing – review & editing, Validation, Resources, Methodology, Investigation, Formal analysis. **Claudia Schormann:** Writing – review & editing, Resources, Methodology, Investigation, Formal analysis. **Evelyn Ullrich:** Writing – review & editing, Validation, Methodology, Investigation, Funding acquisition, Formal analysis. **Leticia Prates Roma:** Writing – review & editing, Validation, Supervision, Methodology, Investigation, Data curation, Conceptualization. **Carsten Kummerow:** Writing – review & editing, Validation, Methodology, Investigation, Formal analysis, Data curation, Conceptualization. **Lorenz Thurner:** Writing – review & editing, Validation, Supervision, Resources, Methodology, Investigation, Funding acquisition, Conceptualization. **Eva C. Schwarz:** Writing – review & editing, Validation, Supervision, Methodology, Investigation, Formal analysis. **Markus Hoth:** Writing – review & editing, Writing – original draft, Validation, Supervision, Project administration, Investigation, Funding acquisition, Data curation, Conceptualization.

Declaration of competing interest

The authors declare that they have no competing interests associated with this manuscript.

Acknowledgements

We very much appreciate the help of Prof. Hermann Eichler and the Institute of Clinical Hemostaseology and Transfusion Medicine, Saarland University and University Medical Center, Homburg, Germany for obtaining human blood cells. We acknowledge Daniela Yildiz from the Department of Molecular Pharmacology (Center for Molecular Signaling (PZMS)) for use of the FACS and particle analysis core facility to obtain a homogenous high fluorescent TMD8-pCasper population (DFG INST 256/508–1). We gratefully acknowledge Kathleen Seelert, Kathrin Förderer, Cora Hoxha and Sandra Janku for cell preparation and help with solutions, ordering, and maintaining a well-functioning lab.

Supplementary materials

Supplementary material associated with this article can be found, in the online version, at doi:10.1016/j.ceca.2025.103091.

Data availability

Data will be made available on request.

References

[1] G. Grynkiewicz, M. Poenie, R.Y. Tsien, A new generation of Ca2+ indicators with greatly improved fluorescence properties, J. Biol. Chem. 260 (1985) 3440–3450. https://www.ncbi.nlm.nih.gov/pubmed/3838314.

[2] A. Miyawaki, J. Llopis, R. Heim, J.M. McCaffery, J.A. Adams, M. Ikura, R.Y. Tsien, Fluorescent indicators for Ca2+ based on green fluorescent proteins and calmodulin, Nature 388 (1997) 882–887, https://doi.org/10.1038/42264.

[3] P. Robinson, A.J. Sparrow, Y. Psaras, V. Steeples, J.N. Simon, C.N. Broyles, Y. F. Chang, F.A. Brook, Y.J. Wang, A. Blease, X. Zhang, Y.A. Abassi, M.A. Geeves, C. N. Toepfer, H. Watkins, C. Redwood, M.J. Daniels, Comparing the effects of chemical Ca(2+) dyes and R-GECO on contractility and Ca(2+) transients in adult and human iPSC cardiomyocytes, J. Mol. Cell Cardiol. 180 (2023) 44–57, https://doi.org/10.1016/j.yjmcc.2023.04.008.

[4] C.S. Gibhardt, A. Vultur, I. Bogeski, Measuring calcium and ROS by genetically encoded protein sensors and fluorescent dyes, Methods Mol. Biol. 1925 (2019) 183–196, https://doi.org/10.1007/978-1-4939-9018-4_17.

[5] N.K. Sinha, C. McKenney, Z.Y. Yeow, J.J. Li, K.H. Nam, T.M. Yaron-Barir, J. L. Johnson, E.M. Huntsman, L.C. Cantley, A. Ordureau, S. Regot, R. Green, The ribotoxic stress response drives UV-mediated cell death, Cell 187 (2024) 3652–3670.e3640, https://doi.org/10.1016/j.cell.2024.05.018.

[6] X. Zhou, K.J. Belavek, M.X. Navarro, K.N. Martinez, A. Hinojosa, E.W. Miller, Ratio-based indicators for cytosolic Ca(2+) with visible light excitation, Proc. Natl. Acad. Sci. U. S. A 122 (2025) e2410436122, https://doi.org/10.1073/pnas.2410436122.

[7] M.D. Bootman, S. Allman, K. Rietdorf, G. Bultynck, Deleterious effects of calcium indicators within cells; an inconvenient truth, Cell Calcium 73 (2018) 82–87, https://doi.org/10.1016/j.ceca.2018.04.005.

[8] N.A. Smith, B.T. Kress, Y. Lu, D. Chandler-Militello, A. Benraiss, M. Nedergaard, Fluorescent Ca(2+) indicators directly inhibit the Na,K-ATPase and disrupt cellular functions, Sci. Signal. 11 (2018), https://doi.org/10.1126/scisignal.aal2039.

[9] N.K. Wolf, D.U. Kissiov, D.H. Raulet, Roles of natural killer cells in immunity to cancer, and applications to immunotherapy, Nat. Rev. Immunol. 23 (2023) 90–105, https://doi.org/10.1038/s41577-022-00732-1.

[10] B.M. Balzasch, A. Cerwenka, Microenvironmental signals shaping NK-cell reactivity in cancer, Eur. J. Immunol. 53 (2023) e2250103, https://doi.org/10.1002/eji.202250103.

[11] K.S. Friedmann, L. Kaschek, A. Knorck, S. Cappello, N. Lunsmann, N. Kuchler, C. Hoxha, G. Schafer, S. Iden, I. Bogeski, C. Kummerow, E.C. Schwarz, M. Hoth, Interdependence of sequential cytotoxic T lymphocyte and natural killer cell cytotoxicity against melanoma cells, J. Physiol. 600 (2022) 5027–5054, https://doi.org/10.1113/JP283667.

[12] L. Kaschek, S. Zophel, A. Knorck, M. Hoth, A calcium optimum for cytotoxic T lymphocyte and natural killer cell cytotoxicity, Semin. Cell Dev. Biol. 115 (2021) 10–18, https://doi.org/10.1016/j.semcdb.2020.12.002.

[13] A. Maul-Pavicic, S.C. Chiang, A. Rensing-Ehl, B. Jessen, C. Fauriat, S.M. Wood, S. Sjoqvist, M. Hufnagel, I. Schulze, T. Bass, W.W. Schamel, S. Fuchs, H. Pircher, C. A. McCarl, K. Mikoshiba, K. Schwarz, S. Feske, Y.T. Bryceson, S. Ehl, ORAI1-mediated calcium influx is required for human cytotoxic lymphocyte degranulation and target cell lysis, Proc. Natl. Acad. Sci. u S. a 108 (2011) 3324–3329, https://doi.org/10.1073/pnas.1013285108.

[14] S. Ganesan, P. Hoglund, Inhibitory receptor crosslinking quantitatively dampens calcium flux induced by activating receptor triggering in NK cells, Front. Immunol. 9 (2018) 3173, https://doi.org/10.3389/fimmu.2018.03173.

[15] S. Ganesan, P. Hoglund, MHC class I molecules co-stimulate NK1.1 signaling and enhance Ca(2+) flux in murine NK cells, Eur. J. Immunol. 51 (2021) 2531–2534, https://doi.org/10.1002/eji.202048709.

[16] C. Grandclement, H. Pick, H. Vogel, W. Held, NK cells respond to haptens by the activation of calcium permeable plasma membrane channels, PLoS. One 11 (2016) e0151031, https://doi.org/10.1371/journal.pone.0151031.

[17] R. Lane, S.O. Ghazi, M.M. Whalen, Increases in cytosolic calcium ion levels in human natural killer cells in response to butyltin exposure, Arch. Environ. Contam. Toxicol. 57 (2009) 816–825, https://doi.org/10.1007/s00244-009-9313-z.

[18] Y. Li, M. Yu, J. Yin, H. Yan, X. Wang, Enhanced calcium signal induces NK cell degranulation but inhibits its cytotoxic activity, J. Immunol. 208 (2022) 347–357, https://doi.org/10.4049/jimmunol.2001141.

[19] A.W.T. MacFarlane, J.F. Oesterling, K.S. Campbell, Measuring intracellular calcium signaling in murine NK cells by flow cytometry, Methods Mol. Biol. 612 (2010) 149–157, https://doi.org/10.1007/978-1-60761-362-6_10.

[20] T. Nguyen, S. Johnston, L. Clarke, P. Smith, D. Staines, S. Marshall-Gradisnik, Impaired calcium mobilization in natural killer cells from chronic fatigue syndrome/myalgic encephalomyelitis patients is associated with transient receptor potential melastatin 3 ion channels, Clin. Exp. Immunol. 187 (2017) 284–293, https://doi.org/10.1111/cei.12882.

[21] T. Nguyen, D. Staines, B. Nilius, P. Smith, S. Marshall-Gradisnik, Novel identification and characterisation of transient receptor potential melastatin 3 ion channels on natural killer cells and B lymphocytes: effects on cell signalling in chronic fatigue syndrome/myalgic encephalomyelitis patients, Biol. Res. 49 (2016) 27, https://doi.org/10.1186/s40659-016-0087-2.

[22] A.M. Shenoy, R.A. Sidner, Z. Brahmi, Signal transduction in cytotoxic lymphocytes: decreased calcium influx in NK cell inactivated with sensitive target cells, Cell Immunol. 147 (1993) 294–301, https://doi.org/10.1006/cimm.1993.1070.

[23] Y. Adib, M. Boy, K. Serror, N. Dulphy, C. des Courtils, L. Duciel, D. Boccara, M. Mimoun, M. Samardzic, M. Bagot, A. Bensussan, L. Michel, Modulation of NK cell activation by exogenous calcium from alginate dressings in vitro, Front. Immunol. 14 (2023) 1141047, https://doi.org/10.3389/fimmu.2023.1141047.

[24] J. Theorell, Y.T. Bryceson, Analysis of intracellular Ca(2+) mobilization in Human NK cell subsets by flow cytometry, Methods Mol. Biol. 1441 (2016) 117–130, https://doi.org/10.1007/978-1-4939-3684-7_10.

[25] M. Van Graft, Y.M. Kraan, I.M. Segers, K. Radosevic, B.G. De Grooth, J. Greve, Flow cytometric measurement of [Ca2+]i and pHi in conjugated natural killer cells and K562 target cells during the cytotoxic process, Cytometry 14 (1993) 257–264, https://doi.org/10.1002/cyto.990140304.

[26] Y.T. Bryceson, M.E. March, H.G. Ljunggren, E.O. Long, Synergy among receptors on resting NK cells for the activation of natural cytotoxicity and cytokine secretion, Blood 107 (2006) 159–166, https://doi.org/10.1182/blood-2005-04-1351.

[27] S.D. Hess, M. Oortgiesen, M.D. Cahalan, Calcium oscillations in human T and natural killer cells depend upon membrane potential and calcium influx, J. Immunol. 150 (1993) 2620–2633. https://www.ncbi.nlm.nih.gov/pubmed/7681076.

[28] Y. Honda, S. Miyazaki, Distinct Ca2+ response patterns in human natural killer cells during induction of necrosis or apoptosis of target cells, Cell Calcium 19 (1996) 297–306, https://doi.org/10.1016/s0143-4160(96)90070-6.

[29] M. Olivas-Aguirre, L.H. Cruz-Aguilar, I. Pottosin, O. Dobrovinskaya, Reduction of Ca(2+) entry by a specific block of KCa3.1 channels optimizes cytotoxic activity of NK cells against T-ALL jurkat cells, Cells 12 (2023), https://doi.org/10.3390/cells12162065.

[30] X. Zhou, K.S. Friedmann, H. Lyrmann, Y. Zhou, R. Schoppmeyer, A. Knorck, S. Mang, C. Hoxha, A. Angenendt, C.S. Backes, C. Mangerich, R. Zhao, S. Cappello, G. Schwar, C. Hassig, M. Neef, B. Bufe, F. Zufall, K. Kruse, B.A. Niemeyer, A. Lis, B. Qu, C. Kummerow, E.C. Schwarz, M. Hoth, A calcium optimum for cytotoxic T

lymphocyte and natural killer cell cytotoxicity, J. Physiol. 596 (2018) 2681–2698, https://doi.org/10.1113/JP274964.
[31] S. Du Preez, N. Eaton-Fitch, P.K. Smith, S. Marshall-Gradisnik, Altered TRPM7-dependent calcium influx in natural killer cells of myalgic encephalomyelitis/Chronic Fatigue Syndrome patients, Biomolecules. 13 (2023), https://doi.org/10.3390/biom13071039.
[32] N. Eaton-Fitch, S. Du Preez, H. Cabanas, K. Muraki, D. Staines, S. Marshall-Gradisnik, Impaired TRPM3-dependent calcium influx and restoration using Naltrexone in natural killer cells of myalgic encephalomyelitis/chronic fatigue syndrome patients, J. Transl. Med. 20 (2022) 94, https://doi.org/10.1186/s12967-022-03297-8.
[33] S.Y. Rah, J.Y. Kwak, Y.J. Chung, U.H. Kim, ADP-ribose/TRPM2-mediated Ca2+ signaling is essential for cytolytic degranulation and antitumor activity of natural killer cells, Sci. Rep. 5 (2015) 9482, https://doi.org/10.1038/srep09482.
[34] Y. Kobayashi, T. Yamashiro, T. Jinnai, A. Nakano, N. Watanabe, T. Kawanishi, H. Tanaka, K. Shigenobu, Target cell-induced calcium signals in human natural killer leukemia cells as revealed by confocal fluorescence microscopy, Exp. Cell Res. 232 (1997) 42–46, https://doi.org/10.1006/excr.1997.3499.
[35] M.A. Cassatella, I. Anegon, M.C. Cuturi, P. Griskey, G. Trinchieri, B. Perussia, Fc gamma R(CD16) interaction with ligand induces Ca2+ mobilization and phosphoinositide turnover in human natural killer cells. Role of Ca2+ in Fc gamma R(CD16)-induced transcription and expression of lymphokine genes, J. Exp. Med. 169 (1989) 549–567, https://doi.org/10.1084/jem.169.2.549.
[36] M. Inngjerdingen, A. Al-Aoukaty, B. Damaj, A.A. Maghazachi, Differential utilization of cyclic ADP-ribose pathway by chemokines to induce the mobilization of intracellular calcium in NK cells, Biochem. Biophys. Res. Commun. 262 (1999) 467–472, https://doi.org/10.1006/bbrc.1999.1234.
[37] A.A. Maghazachi, B.S. Skalhegg, B. Rolstad, A. Al-Aoukaty, Interferon-inducible protein-10 and lymphotactin induce the chemotaxis and mobilization of intracellular calcium in natural killer cells through pertussis toxin-sensitive and -insensitive heterotrimeric G-proteins, FASEB J. 11 (1997) 765–774, https://doi.org/10.1096/fasebj.11.10.9271361.
[38] J. Ng, B.B. Fredholm, M. Jondal, Studies on the calcium dependence of human NK cell killing, Biochem. Pharmacol. 36 (1987) 3943–3949, https://doi.org/10.1016/0006-2952(87)90462-x.
[39] A. Poggi, R. Pardi, N. Pella, L. Morelli, S. Sivori, M. Vitale, V. Revello, A. Moretta, L. Moretta, CD45-mediated regulation of LFA1 function in human natural killer cells. Anti-CD45 monoclonal antibodies inhibit the calcium mobilization induced via LFA1 molecules, Eur. J. Immunol. 23 (1993) 2454–2463, https://doi.org/10.1002/eji.1830231012.
[40] J. Rolin, Z. Al-Jaderi, A.A. Maghazachi, Oxidized lipids and lysophosphatidylcholine induce the chemotaxis and intracellular calcium influx in natural killer cells, Immunobiology 218 (2013) 875–883, https://doi.org/10.1016/j.imbio.2012.10.009.
[41] F.E. Muller, V. Cherkas, G. Stopper, L.C. Caudal, L. Stopper, F. Kirchhoff, C. Henneberger, E.G. Ponimaskin, A. Zeug, Elucidating regulators of astrocytic Ca(2+) signaling via multi-threshold event detection (MTED), Glia 69 (2021) 2798–2811, https://doi.org/10.1002/glia.24070.
[42] E. Vivier, L. Rebuffet, E. Narni-Mancinelli, S. Cornen, R.Y. Igarashi, V.R. Fantin, Natural killer cell therapies, Nature 626 (2024) 727–736, https://doi.org/10.1038/s41586-023-06945-1.
[43] D. Shcherbo, E.A. Souslova, J. Goedhart, T.V. Chepurnykh, A. Gaintzeva, I. I. Shemiakina, T.W. Gadella, S. Lukyanov, D.M. Chudakov, Practical and reliable FRET/FLIM pair of fluorescent proteins, BMC. Biotechnol. 9 (2009) 24, https://doi.org/10.1186/1472-6750-9-24.
[44] C.S. Backes, K.S. Friedmann, S. Mang, A. Knorck, M. Hoth, C. Kummerow, Natural killer cells induce distinct modes of cancer cell death: discrimination, quantification, and modulation of apoptosis, necrosis, and mixed forms, J. Biol. Chem. 293 (2018) 16348–16363, https://doi.org/10.1074/jbc.RA118.004549.
[45] L.A. Blatter, W.G. Wier, Intracellular diffusion, binding, and compartmentalization of the fluorescent calcium indicators indo-1 and fura-2, Biophys. J. 58 (1990) 1491–1499, https://doi.org/10.1016/S0006-3495(90)82494-2.
[46] M. Hoth, C.M. Fanger, R.S. Lewis, Mitochondrial regulation of store-operated calcium signaling in T lymphocytes, J. Cell Biol. 137 (1997) 633–648, https://doi.org/10.1083/jcb.137.3.633.
[47] S. Hollingworth, K.R. Gee, S.M. Baylor, Low-affinity Ca2+ indicators compared in measurements of skeletal muscle Ca2+ transients, Biophys. J. 97 (2009) 1864–1872, https://doi.org/10.1016/j.bpj.2009.07.021.
[48] S. Kahlert, L. Schild, G. Reiser, Mitochondrial polarization in rat hippocampal astrocytes is resistant to cytosolic Ca(2+) loads, J. Neurosci. Res. 66 (2001) 1019–1027, https://doi.org/10.1002/jnr.10052.
[49] A. Quintana, M. Hoth, Apparent cytosolic calcium gradients in T-lymphocytes due to fura-2 accumulation in mitochondria, Cell Calcium 36 (2004) 99–109, https://doi.org/10.1016/j.ceca.2004.01.003.
[50] S. Wrublewsky, J. Glas, C. Carlein, L. Nalbach, M.D.A. Hoffmann, M. Pack, E. A. Vilas-Boas, N. Ribot, R. Kappl, M.D. Menger, M.W. Laschke, E. Ampofo, L. P. Roma, The loss of pancreatic islet NADPH oxidase (NOX)2 improves islet transplantation, Redox. Biol. 55 (2022) 102419, https://doi.org/10.1016/j.redox.2022.102419.
[51] S. Zophel, N. Kuchler, J. Jansky, C. Hoxha, G. Schafer, J.J. Weise, J. Vialle, L. Kaschek, G. Stopper, H. Eichler, D. Yildiz, A. Moter, P. Wendel, E. Ullrich, C. Schormann, T. Rixecker, O. Cetin, F. Neumann, P. Orth, M. Bewarder, M. Hoth, L. Thurner, E.C. Schwarz, CD16+ as predictive marker for early relapse in aggressive B-NHL/DLBCL patients, Mol. Cancer 23 (2024) 210, https://doi.org/10.1186/s12943-024-02123-7.
[52] M. Visa, P.O. Berggren, Sex-dependent intra-islet structural rearrangements affecting alpha-to-beta cell interactions lead to adaptive enhancements of Ca(2+) dynamics in prediabetic beta cells, Diabetologia 67 (2024) 1663–1682, https://doi.org/10.1007/s00125-024-06173-w.
[53] Y. Chen, T. Yang, X. Gu, Y. Chen, Q. Wang, X. Wang, The involvements of intracellular basal calcium and membrane potential in para-phenylenediamine-impaired sperm function, Transl. Androl. Urol. 13 (2024) 2661–2671, https://doi.org/10.21037/tau-24-374.
[54] P.W. Tinning, A. Franssen, S.U. Hridi, T.J. Bushell, G. McConnell, A 340/380 nm light-emitting diode illuminator for Fura-2 AM ratiometric Ca(2+) imaging of live cells with better than 5 nM precision, J. Microsc. 269 (2018) 212–220, https://doi.org/10.1111/jmi.12616.
[55] M. Oheim, M. van 't Hoff, A. Feltz, A. Zamaleeva, J.M. Mallet, M. Collot, New red-fluorescent calcium indicators for optogenetics, photoactivation and multi-color imaging, Biochim. Biophys. Acta 1843 (2014) 2284–2306, https://doi.org/10.1016/j.bbamcr.2014.03.010.
[56] A. Caraux, N. Kim, S.E. Bell, S. Zompi, T. Ranson, S. Lesjean-Pottier, M.E. Garcia-Ojeda, M. Turner, F. Colucci, Phospholipase C-gamma2 is essential for NK cell cytotoxicity and innate immunity to malignant and virally infected cells, Blood 107 (2006) 994–1002, https://doi.org/10.1182/blood-2005-06-2428.
[57] J. Slaats, C.E. Dieteren, E. Wagena, L. Wolf, T.K. Raaijmakers, J.A. van der Laak, C. G. Figdor, B. Weigelin, P. Friedl, Metabolic screening of cytotoxic T-cell effector function reveals the role of CRAC channels in regulating lethal hit delivery, Cancer Immunol. Res. 9 (2021) 926–938, https://doi.org/10.1158/2326-6066.CIR-20-0741.
[58] B. Coiffier, E. Lepage, J. Briere, R. Herbrecht, H. Tilly, R. Bouabdallah, P. Morel, E. Van Den Neste, G. Salles, P. Gaulard, F. Reyes, P. Lederlin, C. Gisselbrecht, CHOP chemotherapy plus rituximab compared with CHOP alone in elderly patients with diffuse large-B-cell lymphoma, N. Engl. J. Med. 346 (2002) 235–242, https://doi.org/10.1056/NEJMoa011795.
[59] M. Pfreundschuh, L. Trumper, A. Osterborg, R. Pettengell, M. Trneny, K. Imrie, D. Ma, D. Gill, J. Walewski, P.L. Zinzani, R. Stahel, S. Kvaloy, O. Shpilberg, U. Jaeger, M. Hansen, T. Lehtinen, A. Lopez-Guillermo, C. Corrado, A. Scheliga, N. Milpied, M. Mendila, M. Rashford, E. Kuhnt, M. Loeffler, G. MabThera International Trial, CHOP-like chemotherapy plus rituximab versus CHOP-like chemotherapy alone in young patients with good-prognosis diffuse large-B-cell lymphoma: a randomised controlled trial by the MabThera International Trial (MInT) Group, Lancet Oncol. 7 (2006) 379–391, https://doi.org/10.1016/S1470-2045(06)70664-7.
[60] A. Knorck, S. Marx, K.S. Friedmann, S. Zophel, L. Lieblang, C. Hassig, I. Muller, J. Pilch, U. Sester, M. Hoth, H. Eichler, M. Sester, E.C. Schwarz, Quantity, quality, and functionality of peripheral blood cells derived from residual blood of different apheresis kits, Transfusion. (Paris) 58 (2018) 1516–1526, https://doi.org/10.1111/trf.14616.
[61] N. Tschorn, Y. van Heuvel, J. Stitz, Transgene expression and transposition efficiency of two-component sleeping beauty transposon vector systems utilizing plasmid or mRNA encoding the transposase, Mol. Biotechnol. 65 (2023) 1327–1335, https://doi.org/10.1007/s12033-022-00642-6.
[62] Y. van Heuvel, S. Schatz, M. Hein, T. Dogra, D. Kazenmaier, N. Tschorn, Y. Genzel, J. Stitz, Novel suspension retroviral packaging cells generated by transposition using transposase encoding mRNA advance vector yields and enable production in bioreactors, Front. Bioeng. Biotechnol. 11 (2023) 1076524, https://doi.org/10.3389/fbioe.2023.1076524.
[63] X. Zhou, S. Zhang, W. Yang, S. Gonder, Z. Sadjadi, N. Piernitzki, A. Moter, S. Sharma, A. Largeot, N. Kuchler, L. Kaschek, G. Schafer, E.C. Schwarz, H. Eichler, E. Ullrich, H. Rieger, O. Staufer, J. Paggetti, E. Moussay, M. Hoth, B. Qu, Restoring NK cell cytotoxicity post-cryopreservation via synthetic cells, Adv. Sci. (Weinh) (2025) e05731, https://doi.org/10.1002/advs.202505731.
[64] C. Kummerow, E.C. Schwarz, B. Bufe, F. Zufall, M. Hoth, B. Qu, A simple, economic, time-resolved killing assay, Eur. J. Immunol. 44 (2014) 1870–1872, https://doi.org/10.1002/eji.201444518.